THE ASTROPHYSICAL JOURNAL SUPPLEMENT SERIES, 119:207–238, 1998 December

A HIGH-DISPERSION SPECTROSCOPIC SURVEY OF THE HOT WHITE DWARFS: THE *IUE* NEWSIPS SWP ECHELLE DATA SET

J. B. HOLBERG,[1] M. A. BARSTOW,[2] AND E. M. SION[3]
Received 1998 April 16; accepted 1998 July 13

ABSTRACT

This paper summarizes the results obtained from a comprehensive analysis of all of the SWP echelle spectra of the white dwarf stars contained in the *IUE* Final Archive. A total of 209 NEWSIPS spectra of 55 degenerate stars of various types have been systematically reduced and analyzed. These include, in addition to conventional white dwarfs, several examples of the hot planetary nebula central stars such as NGC 246, which represent the initial stages of He-rich degenerate evolution. A representative summary of the stellar, circumstellar, and interstellar features found to be present in these spectra is presented. For 33 of the 55 stars, multiple spectra of sufficient quality exist so that co-added spectra with improved signal-to-noise ratio can be constructed. Much previously unrecognized detail and many new features are evident in these data. In addition, it was found necessary to apply several corrections to the NEWSIPS extracted spectra. These corrections, involving the wavelength scale and flux uncertainty vector, are described.

Subject headings: surveys — ultraviolet: stars — white dwarfs

1. INTRODUCTION

The ability of *IUE* to obtain high-dispersion UV spectra of such relatively faint stars as hot white dwarfs routinely has produced a number of remarkable discoveries involving narrow interstellar-like lines. These discoveries have opened up several new areas of investigation. These areas include the patterns of trace element abundance observed in white dwarf photospheres and the resulting implications for the chemical evolution of white dwarf atmospheres. Related to this are investigations of processes such as diffusion, radiative levitation, mass loss, and accretion, which control the composition of white dwarf atmospheres and which may also lead to the creation of unique circumstellar environments. Virtually all these areas have been the exclusive domain of UV spectroscopy, and *IUE* has played a major role over the past two decades in contributing to our understanding of these processes.

Initially, Bruhweiler & Kondo (1981) sought to obtain SWP echelle spectra of several hot white dwarfs in order to use the supposedly featureless continua of these stars as a means of studying absorption lines in the local ISM. Although the expected ISM features were seen, several white dwarfs showed some surprising absorption features due to highly ionized species such as N V, Si IV, and C IV. These ions are not frequently seen over the short (<100 pc) interstellar distances to nearby white dwarfs. Equally surprising was the discovery in the *IUE* echelle spectra of several cooler stars, of Si II and Si III transitions having excited lower levels (Bruhweiler & Kondo 1983). In addition, the existence of such heavy elements in the optical spectra of hot white dwarfs was virtually unknown at the time. The existence of heavy elements in the photospheres of the pure-hydrogen DA white dwarfs was regarded as improbable because of the relatively short residence times of heavy species in the high gravitational field of a degenerate star. Theoretical calculations (Vauclair, Vauclair, & Greenstein 1979, and others) had shown that certain ions could be levitated by radiation pressure, but there existed little observational verification that this actually occurred. These and other considerations first led Bruhweiler & Kondo (1981) to propose that highly ionized species occurred in a zone of circumstellar ionization produced by the strong EUV and UV radiation fields of the hottest of these stars. The photospheric nature of these narrow interstellar-like lines in at least one star was established by Dupree & Raymond (1982), who demonstrated that some of these features shared the orbital velocity of the white dwarf component of the Feige 24 system, while other features appeared to remain stationary. Since that time, the interstellar-like lines have been discovered in a number of other degenerate stars and have been variously interpreted as photospheric, circumstellar, and interstellar in origin. It is clear now that all three circumstances exist, and good examples of each can be found in the *IUE* Final Archive. Further, *IUE* observations now show that, although radiative levitation is important in explaining the presence of heavy elements in the atmospheres of some white dwarfs, there must be other physical processes such as mass loss and accretion that operate over a wide range of stellar temperatures and gravities.

The collection of white dwarf echelle data in the *IUE* Final Archive is an important legacy of the *IUE* program. These data presently provide the most complete inventory of the chemical content of white dwarf atmospheres, extending over virtually all species of hot white dwarfs. The study of the chemical composition of hot white dwarf photospheres has emerged as one of the major areas of study in white dwarf astrophysics and has helped shape our understanding of how white dwarfs evolve from the post–planetary nebula stage to cool, fully degenerate white dwarfs. In the broadest terms, it still remains unclear why nature produces two apparently distinct spectral types of white dwarf, the H-rich DA stars and the He-rich DB and DO stars and why the relative numbers of these two spec-

[1] Lunar & Planetary Laboratory, University of Arizona, Gould-Simpson Building, Tucson AZ 85721; holberg@argus.lpl.arizona.edu.
[2] Department of Physics & Astronomy, University of Leicester, University Road, Leicester, LE1 7RH, England; mab@star.le.ac.uk.
[3] Department of Astronomy & Astrophysics, Villanova University, Villanova, PA 19085; emsion@ucis.vill.edu.

troscopic classes appear to change as white dwarfs cool. It could be that this dichotomy in spectral type is primordial, with the dominant H or He content of the photosphere fixed late in the planetary nebulae central star stage, or it could be that most white dwarfs evolve in an essentially similar fashion and the chemical composition of their thin photospheres changes as the stars cool. *IUE* has helped to provide clear evidence for the evolution of the heavy element content in DA white dwarf atmospheres. The most metal-rich white dwarfs are almost always the hottest, and this heavy element content falls dramatically as stars cool below 50,000 K (Barstow et al. 1993; Marsh et al. 1997). This helps to explain a key aspect of the observed soft X-ray and EUV fluxes from hot DA white dwarfs: namely, the dramatically depressed flux levels due to high short-wavelength opacities in the hottest of these stars. It was the high levels of heavy elements, in particular Fe and Ni, measured in *IUE* echelle spectra that helped to establish the link between the short-wavelength opacity and the heavy element photospheric content (Tweedy 1993; Holberg et al. 1993).

In spite of relatively low spectral resolution ($\lambda/\Delta\lambda = 10{,}000$), *IUE* has also contributed to the study of the local interstellar medium (LISM) by providing numerous sources of nearby, clean UV stellar continuum with which to probe the LISM within 100 pc of the Sun. The nearby white dwarfs in the *IUE* Final Archive constitute a significant global sample of LISM sight lines with which to study mean velocities and column densities for such key species as N I, C II, O I, Si II, and S II. These column densities can often be combined with directly measured H and He column densities, obtained from EUV observations of these same stars, to establish accurate relative abundances and to provide information on the ionization state of the LISM.

The extensive nature of the *IUE* Final Archive also makes it an ideal starting point for planning future UV observations of hot white dwarfs using the Space Telescope Imaging Spectrometer (STIS) on the *Hubble Space Telescope* (*HST*), or observations in the 900–1200 Å region with the soon-to-be launched *Far Ultraviolet Spectroscopic Explorer* (*FUSE*) mission. Critical information regarding both the presence or absence of various species and the expected stellar and interstellar velocity components are now available for a number of specific key objects. These stars can also serve as a representative set of comparison objects for previously unobserved stars. Finally, on a utilitarian level, the challenge posed by the weakly exposed, relatively low signal-to-noise ratio (S/N) white dwarf spectra has required the development of reduction and analysis techniques which help to maximize the information extracted from *IUE* echelle data in general.

More than 50 publications have resulted from *IUE* high-dispersion observations of hot white dwarfs. One of the most notable is Tweedy (1991), which presents some of the first co-additions of *IUE* echelle spectra for white dwarfs and led to the discovery of many previously overlooked features. This originally inspired much of the co-addition work presented in this paper. Another important paper is that of Vennes, Thejll, & Shipman (1991, hereafter VTS). Although these authors considered only single spectra, they investigated a wide range of hot white dwarfs, finding several stars with evidence of interstellar-like features and placing limits on the photospheric C, N, and Si content in many more. In spite of the attention paid to many individual stars over the years, the data set as a whole has never been systematically analyzed nor have several useful techniques for enhancing the data, such as co-addition, been used to their full potential. Most importantly, virtually all prior work has employed the original *IUE* data processing system, IUESIPS. Much of this prior work on white dwarf echelle spectra is reviewed in Holberg (1995) and Holberg, Barstow, & Sion (1998c).

In planning the construction of an *IUE* Final Archive, considerable effort went into the development of improved techniques for processing *IUE* camera images and for extracting spectra. New, enhanced geometrical and photometric corrections and calibrations were developed. These improvements, based on years of experience with *IUE* data, were incorporated into the NEWSIPS processing system described in Nichols & Linsky (1996). With regard to SWP echelle data, the chief improvements were (1) a greatly improved interorder background subtraction, which helped to correct a long-standing problem with the extracted fluxes in the highest orders; (2) a substantially better defined intensity transfer function (ITF), used to linearize the camera response; (3) a uniform processing of the entire data set, which corrected a number of previous errors in the wavelength scale and ITF; and (4) the inclusion of an explicit flux uncertainty vector, which can be used to characterize errors in measured quantities such as the centroids and equivalent widths of observed lines. Among the expected benefits resulting from all of these changes and enhancements is a significant increase in spectral (S/N) and a more uniform, better characterized data set.

In this paper we describe a comprehensive analysis of the entire set of *IUE* SWP echelle spectra for degenerate stars in the *IUE* Final Archives. All existing white dwarf spectra have been extracted and examined to determine if a useful signal is present. For those stars possessing significant signal levels, we have attempted to measure the majority of the real spectral features present. This work should provide a good starting point for those wishing to further investigate the large body of existing high-dispersion UV spectra of degenerate stars. In § 2 we present a log of the data and a brief description of the observations. Reduction procedures are described in § 3. In § 4 examples of spectra from several stellar types exhibiting various phenomena are presented, and tabulated lists of the stellar, circumstellar and interstellar features found in the data are presented. A preliminary discussion of a small part of the NEWSIPS analysis presented in this paper is contained in Holberg, Barstow, & Sion (1998d).

2. THE *IUE* DATA SET

More than 50 hot degenerate stars were observed with the *IUE* SWP camera in its echelle mode during its 18.5 yr of operation. All the major white dwarf categories were targeted: the H-rich DA stars, the He-rich DO and DB stars, and H-He spectral hybrids, the DAO stars. In our study of white dwarf spectra we also include very hot, He-rich, objects such as PG 1159−035 as well as several key planetary nebula central stars such as NGC 246, K1-16, and RXJ 2117.1+3412. Although some important targets would have profited from additional or better observations, the majority of the known white dwarfs bright enough ($V < 14.5$) and hot enough ($T_{\rm eff} > 15{,}000$ K) to be observed in the SWP echelle mode were eventually observed at least once. These observations, involving many observers over

TABLE 1

WHITE DWARF PARAMETERS

WD Number	Alternate Name	Type	V	$T_{\rm eff}$ (K)	log g	References
		H-rich Degenerates				
WD 0004+330.....	GD 2	DA1	13.85	49,360	7.63	1
WD 0050−332.....	GD 659	DA1.5	13.36	36,000	7.68	2
WD 0134+833.....	GD 419	DA2.5	13.11	18,300	7.94	1
WD 0205+250.....	EG 15	DA2.5	13.22	20,000	7.7	3
WD 0232+035.....	Feige 24	DA1+dMe	12.25	62,950	7.20	4
WD 0343−007.....	KUV 343-7	DA1	14.91	65,780	7.67	1
WD 0346−011.....	GD 50	DAO1	14.06	43,200	9.2	4
WD 0347+171.....	V 471 Tau	DA1.5+K2 V	13.64	32,400	8.27	5
WD 0413−077.....	40 Eri B	DA3	9.51	16,400	7.85	6
WD 0441+467.....	S 216	DAO1	12.67	83,800	7.17	7
WD 0455−282.....	REJ 0457−281	DA1	13.95	57,200	7.88	4
WD 0501+527.....	G191-B2B	DA1	11.73	56,000	7.5	8
WD 0512+326.....	KW Aur C	DA1+F4 V	13.9	42,200	...	9
WD 0518−105.....	REJ 0521−102	DA1.5	15.89	33,000	8.7	4
WD 0549+158.....	GD 71	DA1.5	13.03	32,750	7.68	1
WD 0612+177.....	EG 46	DA2	13.37	25,165	7.83	1
WD 0621−376.....	REJ 0623−374	DA1	12.09	60,300	7.34	10
WD 0642−166.....	Sirius B	DA2+AO V	8.44	24,790	8.57	11
WD 0644+375.....	EG 50	DA2.5	12.05	21,000	8.04	1
WD 1013−050.....	REJ 1016−053	DAO+dMe	14.21	56,400	7.74	7
WD 1031−114.....	EG 70	DA2	13.02	25,800	7.94	4
WD 1134+300.....	GD 140	DA2	12.49	21,700	8.5	3
WD 1148−230.....	EC 1148-2	DAO	11.76	>50,000	8	...
WD 1202+608.....	Feige 55	DAO+D?	13.61	58,300	7.15	7
WD 1210+533.....	PG 1210+533	DAO1	14.12	44,800	7.89	7
WD 1234+481.....	HS 1234+481	DA1	14.42	56,400	7.67	1
WD 1254+223.....	GD 153	DA1.5	13.35	38,686	7.66	1
WD 1302+597.....	GD 323	DAB1.5	14.52	28,750	8	12
WD 1314+293.....	HZ 43	DA1	12.91	50,560	7.95	13
WD 1337+705.....	EG 102	DA2.5	12.77	20,230	7.9	6
WD 1615−154.....	EG 118	DA1.5	13.42	29,732	7.94	6
WD 1620−391.....	CD −38°10980	DA2	11.01	24,800	8.05	2
WD 1631+781.....	REJ 1629+780	DA1+dMe	14.1	44,560	7.79	1
WD 1800+685.....	KUV	DA1	14.72	46,000	7.68	4
WD 1845+019.....	Lanning 18	DA1.5	12.95	29,450	7.84	1
WD 2004−605.....	REJ 2009−602	DA1	13.59	44,200	8.14	14
WD 2028+390.....	GD 391	DA2	13.39	24,300	7.89	1
WD 2032+248.....	Wolf 1346	DA2.5	11.53	20,000	7.9	15
WD 2111+498.....	GD 394	DA1.5	13.09	37,360	7.83	16
WD 2117+539.....	G231−40	DA3.5	12.33	14,490	7.85	6
WD 2211−495.....	REJ 2214−491	DA1	11.71	63,500	7.5	10
WD 2309+105.....	GD 246	DA1	13.10	58,700	7.81	1
WD 2331−475.....	REJ 2334−471	DA1	13.44	55,800	8.07	1
WD 2350−706.....	HD 223816B	DA1+F5 IV	14.4	69,300	8	17
		He-rich Degenerates				
WD 0005+511.....	KPD 0005+5106	DO	13.32	120,000	7	18
WD 0044−121.....	NGC 246	PNN	13.40	150,000	5.7	18
WD 0112+104.....	PG 0112+104	DB1.5	15.36	30,800	7.8	...
WD 0501−289.....	REJ 0503−289	DO	13.90	70,000	7.5	18
WD 1034+001.....	PG 1034+001	DO	13.22	100,000	7.5	18
WD 1159−034.....	PG 1159−035	PG 1159	14.87	140,000	7	18
WD 1211+332.....	HZ 21	DO2	14.22	53,000	7.8	18
WD 1634−573.....	HD 149499B	DO+KO V	11.7	49,500	8	19
WD 1645+325.....	GD 358	DB2	13.62	27,000	8	20
WD 1821+643.....	K1-16	PG 1159	15.04	140,000	6.1	18
WD 2117+342.....	RXJ 2117.1+341	PG 1159	13.16	170,000	6	18

REFERENCES.—(1) Finley, Koester, & Basri 1997; (2) Holberg et al. 1995a, HBA; (3) Kidder 1991; (4) Vennes et al. 1997; (5) Barstow et al. 1997; (6) Bergeron, Saffer, & Liebert 1992; (7) Bergeron et al. 1994; (8) Lanz et al. 1996; (9) Vennes et al. 1998; (10) Holberg et al. 1993; (11) Holberg et al. 1998a; (12) Koester et al. 1994; (13) Barstow, Holberg, & Koester 1995; (14) Marsh et al. 1997; (15) HBG; (16) Barstow et al. 1996; (17) Barstow et al. 1994a; (18) Werner et al. 1997; (19) Jordan et al. 1997; (20) Provencal et al. 1996.

the entire lifetime of *IUE*, represent a considerable effort. The average exposure time for all white dwarf SWP echelle images is in excess of 5 hr. Reaching the faintest (and often most interesting stars) frequently required multiple shift VILSPA/Goddard exposures of up to 18 hr.

Several years ago a NASA Astrophysical Data Analysis program was undertaken with the goal of analyzing the entire SWP echelle data set for the white dwarf stars. This program initially worked only with the IUESIPS versions of the spectra but was expanded to include work with the

TABLE 2

LOG OF *IUE* SWP ECHELLE SPECTRA

WD Number	SWP Number	Aperture	Date	Exposure (s)	C/B	Shift (mÅ)	Observer	Status
WD 0004+330.....	27176	L	1985 Nov 26	24000	156/88	0.0	Bruhweiler	Z
WD 0050−332.....	18289	L	1982 Oct 14	24000	163/98	−8.8	Basri	Z
WD 0050−332.....	28384	L	1986 May 27	22200	180/100	−10.0	Bruhweiler	Z
WD 0050−332.....	52116	L	1994 Sep 14	20096	129/84	+2.0	Holberg	Z
WD 0050−332.....	52129	L	1994 Sep 15	20096	138/89	+23.5	Holberg	Z
WD 0050−332.....	52137	L	1994 Sep 17	20996	132/84	−2.7	Holberg	Z
WD 0134+833.....	27188	L	1985 Nov 28	25019	148/102	0.0	Vauclair	NS
WD 0205+250.....	23647	L	1984 Aug 9	24600	180/87	0.0	Bruhweiler	Z
WD 0232+035.....	16292	L	1982 Feb 8	25200	235/113	+22.4	Raymond	Z
WD 0232+035.....	18216	L	1982 Oct 5	9899	130/51	+14.0	Bruhweiler	Z
WD 0232+035.....	20614	L	1983 Aug 5	10800	133/52	−3.5	Dupree	Z
WD 0232+035.....	23474	L	1984 Jul 19	14400	163/60	+42.6	Dupree	Z
WD 0232+035.....	25163	S	1985 Feb 3	18600	183/107	+41.2	Raymond	Z
WD 0232+035.....	42084	L	1991 Jul 17	21600	191/56	+48.4	Vennes	Z
WD 0232+035.....	42089	L	1991 Jul 18	22080	196/61	+34.4	Vennes	Z
WD 0232+035.....	42095	L	1991 Jul 19	22200	255/61	+20.8	Vennes	Z
WD 0232+035.....	42105	L	1991 Jul 20	25500	209/67	+43.5	Vennes	Z
WD 0232+035.....	42128	L	1991 Jul 26	22200	203/62	+40.4	Vennes	Z
WD 0232+035.....	52127	L	1994 Sep 15	10800	117/62	−43.5	Vennes	Z
WD 0232+035.....	52128	L	1994 Sep 15	9000	103/53	−37.7	Vennes	Z
WD 0232+035.....	52156	L	1994 Sep 19	10800	116/54	−42.0	Vennes	Z
WD 0232+035.....	52157	L	1994 Sep 19	7200	88/32	+8.4	Vennes	Z
WD 0343−007.....	43400	S	1991 Dec 16	4199	66/29	0.0	Finley	NS
WD 0346−011.....	31976	L	1987 Oct 3	46799	225/163	0.0	Holberg	Z
WD 0347+171.....	15898	L	1981 Dec 28	10800	88/50	+5.0	Beavers	Z
WD 0347+171.....	15899	L	1981 Dec 29	6840	64/38	...	Beavers	Z
WD 0347+171.....	15900	L	1981 Dec 29	12360	83/53	+8.0	Beavers	Z
WD 0347+171.....	28826	L	1986 Aug 4	15000	107/73	...	Sion	Z
WD 0347+171.....	31611	L	1987 Aug 22	11400	109/58	...	Sion	Z
WD 0347+171.....	31630	L	1987 Aug 23	23453	152/99	+17.0	Bruhweiler	Z
WD 0347+171.....	32649	L	1988 Jan 1	11160	80/48	...	Guinan	Z
WD 0347+171.....	32659	L	1988 Jan 3	13020	91/55	...	Guinan	Z
WD 0347+171.....	37928	L	1989 Dec 31	15000	87/54	−32.0	Mullan	Z
WD 0347+171.....	42193	L	1991 Aug 7	9420	68/37	−6.0	Hakala	Z
WD 0413−077.....	7972	L	1980 Feb 17	13200	255/84	+10.87	Greenstein	Z
WD 0413−077.....	14416	L	1981 Jul 7	5220	161/46	−11.70	Bruhweiler	Z
WD 0413−077.....	49058	L	1993 Oct 31	5400	155/47	−98.25	Shipman	Z
WD 0413−077.....	49059	L	1993 Oct 31	5400	147/46	+132.60	Shipman	Z
WD 0413−077.....	49060	L	1993 Nov 1	5880	159/50	+144.20	Shipman	Z
WD 0413−077.....	49143	L	1993 Nov 7	6000	164/50	−87.70	Shipman	Z
WD 0413−077.....	49144	L	1993 Nov 8	5400	150/47	+158.25	Shipman	Z
WD 0413−077.....	49190	L	1993 Nov 10	6000	170/61	+57.90	Shipman	Z
WD 0413−077.....	49191	L	1993 Nov 10	6000	166/51	+45.90	Shipman	Z
WD 0413−077.....	49192	L	1993 Nov 11	5100	155/45	−46.45	Shipman	Z
WD 0441+467.....	27558	L	1986 Jan 22	18900	210/109	+16.2	Fesen	Z
WD 0441+467.....	43949	L	1992 Feb 8	21299	171/57	+19.2	Gonzalez	Z
WD 0441+467.....	56071	L	1995 Oct 12	21600	204/125	−14.5	Napiwotzki	Z
WD 0441+467.....	56072	L	1995 Oct 12	21600	171/989	−17.8	Napiwotzki	Z
WD 0455−282.....	46304	L	1992 Nov 19	37200	186/124	−2.6	Holberg	Z
WD 0455−282.....	56213	L	1995 Nov 18	45000	197/137	+26.1	Barstow	Z
WD 0455−282.....	56262	L	1995 Dec 2	47160	232/150	−15.3	Barstow	Z
WD 0455−282.....	56267	L	1995 Dec 4	39100	255/123	−5.3	Barstow	Z
WD 0501+527.....	13541	L	1981 Mar 21	4800	116/36	+3.5	Bruhweiler	Z
WD 0501+527.....	18217	L	1982 Oct 6	6000	128/48	−34.7	Bruhweiler	Z
WD 0501+527.....	22428	L	1984 Mar 6	4800	145/84	−15.5	Bruhweiler	Z
WD 0501+527.....	41183	L	1991 Mar 26	7799	148/41	+29.0	Carini	Z
WD 0501+527.....	41207	L	1991 Mar 29	7500	146/41	+11.5	Monier	Z
WD 0501+527.....	41281	L	1991 Apr 3	9600	171/49	−20.7	Rawley	Z
WD 0501+527.....	41301	L	1991 Apr 5	19200	253/98	−7.8	Pitts	Z
WD 0501+527.....	46600	L	1992 Dec 27	10500	175/48	+6.4	Pitts	Z
WD 0501+527.....	46693	L	1993 Jan 9	10500	184/56	+15.0	Newmark	Z
WD 0501+527.....	46677	L	1993 Jan 7	5700	150/41	−4.8	Weinstein	Z
WD 0501+527.....	48544	S	1993 Sep 6	14996	113/66	+24.6	Sion	Z
WD 0501+527.....	52405	L	1994 Oct 14	10799	174/53	+4.3	Rawley	Z
WD 0501+527.....	52677	L	1994 Oct 28	9899	172/51	+19.0	England	Z
WD 0501+527.....	55664	L	1995 Aug 23	9597	170/53	−16.4	Nichols	Z
WD 0512+326.....	45663	L	1992 Sep 17	22800	203/90	+43.9	Guinan	Z
WD 0512+326.....	47384	L	1993 Mar 29	24000	175/100	−8.7	Etzel	Z
WD 0512+326.....	50435	L	1994 Mar 31	18296	140/81	−24.7	Guinan	Z
WD 0518−105.....	45949	L	1992 Oct 15	2040	34/18	−24.2	Marsh	NS
WD 0549+158.....	18273	L	1982 Oct 13	22200	163/96	+3.1	Basri	Z
WD 0549+158.....	22023	L	1984 Jan 16	22500	168/65	+1.8	Bruhweiler	Z

TABLE 2—*Continued*

WD Number	SWP Number	Aperture	Date	Exposure (s)	C/B	Shift (mÅ)	Observer	Status
WD 0549+158.....	49873	L	1994 Jan 22	20699	160/96	−9.6	Holberg	Z
WD 0612+177.....	23953	L	1984 Sep 13	19800	120/76	0.0	Bruhweiler	Z
WD 0612+177.....	42921	L	1991 Oct 27	44099	196/139	0.0	Holberg	NS
WD 0612+177.....	44002	L	1992 Feb 16	43199	190/123	0.0	Holberg	Z
WD 0621−376.....	45951	L	1992 Oct 15	14400	190/64	−111.2	Holberg	Z
WD 0621−376.....	47985	L	1993 Jun 28	11399	77/53	0.0	Vennes	NS
WD 0621−376.....	49037	L	1993 Oct 29	6000	184/55	−16.0	Marsh	Z
WD 0621−376.....	49038	L	1993 Oct 29	12598	177/53	+45.8	Holberg	Z
WD 0621−376.....	49039	L	1993 Oct 30	12598	174/64	+77.5	Holberg	Z
WD 0642−166.....	2706	S	1978 Sep 20	20	35/19	0.0	Böhm-Vitense	NS
WD 0642−166.....	2730	L	1978 Sep 22	600	255/143	0.0	Böhm-Vitense	B
WD 0642−166.....	2750	L	1978 Sep 24	600	207/44	+179.5	Böhm-Vitense	Z
WD 0642−166.....	10072	L	1980 Sep 10	3	36/19	0.0	Savedoff	NS
WD 0642−166.....	10075	S	1980 Sep 10	1200	160/41	+37.1	Savedoff	Z
WD 0642−166.....	22693	S	1984 Apr 8	1200	78/25	−11.3	Gry	Z
WD 0642−166.....	22694	S	1984 Apr 8	1200	74/26	−25.9	Gry	Z
WD 0644+375.....	13779	L	1981 Apr 22	20700	188/108	0.0	Raymond	Z
WD 1013−050.....	47721	L	1993 May 24	20696	126/84	−2.3	Vennes	Z
WD 1013−050.....	49832	L	1994 Jan 14	23399	177/129	0.0	Vennes	Z
WD 1013−050.....	49885	L	1994 Jan 24	22500	150/105	+2.1	Vennes	Z
WD 1031−114.....	33807	L	1988 Jun 24	23100	147/94	0.0	Holberg	Z
WD 1134+300.....	23374	L	1984 Jul 1	14099	107/40	0.0	Bruhweiler	Z
WD 1148−230.....	48112	L	1993 Jul 14	5699	96/42	0.0	Sion	Z
WD 1202+608.....	31178	L	1987 Jun 17	26700	116/185	−6.9	Green	Z
WD 1202+608.....	49841	L	1994 Jan 17	20097	207/147	+21.2	Holberg	Z
WD 1202+608.....	49844	L	1994 Jan 18	22800	235/182	−10.6	Holberg	Z
WD 1202+608.....	49859	L	1994 Jan 21	19500	242/189	+0.2	Holberg	Z
WD 1202+608.....	50171	L	1994 Mar 6	24000	156/90	−2.0	Tweedy	Z
WD 1202+608.....	53873	L	1995 Feb 9	24000	157/100	−14.5	Holberg	Z
WD 1202+608.....	53930	L	1995 Feb 17	24600	178/120	+5.1	Holberg	Z
WD 1202+608.....	54495	L	1995 Apr 24	22197	159/92	+11.8	Holberg	Z
WD 1210+533.....	31277	L	1987 Jul 1	46799	222/152	0.0	Holberg	Z
WD 1234+481.....	39161	L	1990 Jun 29	32519	128/76	0.0	Koester	Z
WD 1254+223.....	20369	L	1983 Jul 3	21720	142/82	+21.5	Bruhweiler	Z
WD 1254+223.....	22192	L	1984 Feb 3	20396	135/78	−21.5	Finley	Z
WD 1302+597.....	40123	L	1990 Nov 16	50399	180/145	0.0	Sion	B
WD 1302+597.....	43344	L	1991 Dec 8	57599	178/124	0.0	Sion	Z
WD 1314+293.....	13689	L	1981 Apr 9	25200	186/88	+0.6	Basri	Z
WD 1314+293.....	27225	S	1985 Dec 5	21600	52/132	—	York	Z
WD 1314+293.....	49958	L	1994 Feb 4	17819	156/88	−1.4	Holberg	Z
WD 1314+293.....	49963	L	1994 Feb 5	19977	159/94	−14.6	Holberg	Z
WD 1314+293.....	50068	L	1994 Feb 20	23085	209/115	+15.7	Demartino	Z
WD 1337+705.....	17182	L	1982 Jun 10	26279	155/100	0.0	Bruhweiler	Z
WD 1615−154.....	16364	L	1982 Feb 18	24000	164/104	0.0	Bruhweiler	Z
WD 1620−391.....	18290	L	1982 Oct 15	7200	147/47	−1.8	Basri	Z
WD 1620−391.....	25669	L	1985 Apr 12	7200	141/42	−14.3	Holberg	Z
WD 1620−391.....	40922	L	1991 Feb 23	7500	142/39	−23.2	Mansperger	Z
WD 1620−391.....	41346	L	1991 Apr 11	8100	142/39	−10.7	Demartino	Z
WD 1620−391.....	41379	L	1991 Apr 14	10500	171/46	+2.1	Fernley	Z
WD 1620−391.....	41435	L	1991 Apr 20	10800	192/55	+21.5	Rawley	Z
WD 1620−391.....	41466	L	1991 Apr 24	12000	178/52	+8.5	Demartino	Z
WD 1620−391.....	41467	L	1991 Apr 24	5939	112/35	+2.7	Demartino	Z
WD 1620−391.....	41495	L	1991 Apr 27	21600	255/91	−7.5	Mansperger	Z
WD 1620−391.....	42260	L	1991 Aug 15	12000	190/53	+19.3	Monier	Z
WD 1620−391.....	42297	L	1991 Aug 20	6780	129/34	+3.4	Demartino	Z
WD 1620−391.....	42309	L	1991 Aug 22	8340	146/37	+7.0	Demartino	Z
WD 1620−391.....	47010	L	1993 Feb 20	10200	170/59	−10.5	England	Z
WD 1620−391.....	47273	L	1993 Mar 13	9000	169/66	−25.6	Newmark	Z
WD 1620−391.....	48308	L	1993 Aug 5	10800	173/62	+16.9	Mansperger	Z
WD 1620−391.....	50517	L	1994 Apr 10	9000	186/103	+4.2	Teays	Z
WD 1620−391.....	51681	L	1994 Aug 1	10800	179/68	−10.4	Rawley	Z
WD 1620−391.....	51794	L	1994 Aug 13	10800	177/73	+4.8	England	Z
WD 1631+781.....	42033	L	1991 Jul 10	23700	143/49	−3.8	Sion	Z
WD 1631+781.....	44010	L	1992 Feb 17	26400	154/86	+22.5	Holberg	Z
WD 1631+781.....	49563	L	1993 Dec 10	24300	158/99	−16.7	Sion	Z
WD 1800+685.....	57789	L	1996 Aug 13	42000	180/126	−1.4	Barstow	Z
WD 1800+685.....	57791	L	1996 Aug 14	42000	192/123	+0.9	Barstow	Z
WD 1800+685.....	57793	L	1996 Aug 15	42000	220/126	+0.5	Barstow	Z
WD 1845+019.....	34660	L	1988 Nov 1	22500	152/87	0.0	Holberg	Z
WD 2004−605.....	49050	L	1993 Oct 30	31194	200/128	0.0	Holberg	Z
WD 2028+390.....	20842	L	1983 Aug 30	23399	144/80	0.0	Bruhweiler	Z
WD 2032+248.....	13542	L	1981 Mar 21	15000	181/101	+19.9	Bruhweiler	Z
WD 2032+248.....	14415	L	1981 Jul 7	15000	148/60	−22.3	Bruhweiler	Z

TABLE 2—*Continued*

WD Number	SWP Number	Aperture	Date	Exposure (s)	C/B	Shift (mÅ)	Observer	Status
WD 2032+248.....	52152	L	1994 Sep 18	24600	202/101	−1.8	Holberg	Z
WD 2032+248.....	52167	L	1994 Sep 20	25620	210/113	+28.4	Holberg	Z
WD 2032+248.....	52175	L	1994 Sep 21	24600	224/102	−21.6	Holberg	Z
WD 2111+498.....	16891	L	1982 May 5	18000	132/52	+20.3	Bruhweiler	Z
WD 2111+498.....	22754	L	1984 Apr 15	23399	180/101	+7.2	Bruhweiler	Z
WD 2111+498.....	49756	L	1994 Jan 3	19376	133/87	−30.3	Holberg	Z
WD 2111+498.....	49758	L	1994 Jan 4	20696	181/87	+1.5	Holberg	Z
WD 2117+539.....	25184	L	1985 Feb 6	24900	170/124	0.0	Bruhweiler	Z
WD 2211−495.....	44766	L	1992 May 25	7200	169/44	−12.0	Sion/Holberg	Z
WD 2211−495.....	44767	L	1992 May 25	7200	167/45	−18.0	Sion	Z
WD 2211−495.....	47954	L	1993 Jun 25	7200	182/42	+122.6	Holberg	Z
WD 2211−495.....	47955	L	1993 Jun 25	7200	158/44	+28.4	Holberg	Z
WD 2211−495.....	47956	L	1993 Jun 25	7200	195/109	+16.9	Holberg	Z
WD 2211−495.....	47996	L	1993 Jun 29	7200	161/43	−19.0	Holberg	Z
WD 2309+105.....	17010	L	1982 May 21	24000	193/106	−2.1	Basri	Z
WD 2309+105.....	46544	L	1992 Dec 20	21900	170/93	+8.2	Vennes/Chayer	Z
WD 2309+105.....	46546	L	1992 Dec 21	24300	174/94	+5.5	Vennes/Chayer	Z
WD 2309+105.....	46560	L	1992 Dec 22	25500	210/119	−11.4	Vennes/Chayer	Z
WD 2309+105.....	46723	L	1993 Jan 13	22200	166/95	+46.2	Vennes	Z
WD 2331−475.....	44778	L	1992 May 25	26399	155/91	+124.2	Sion	Z
WD 2331−475.....	47877	L	1993 Jun 16	23399	124/93	...	Barstow/Sion	NS
WD 2331−475.....	47964	L	1993 Jun 26	23700	136/96	...	Vennes	NS
WD 2331−475.....	47974	L	1993 Jun 27	22500	139/94	...	Vennes	Z
WD 2331−475.....	47993	L	1993 Jun 28	25200	145/100	+44.3	Holberg	Z
WD 2331−475.....	48186	L	1993 Jul 20	23399	183/95	−121.6	Vennes	Z
WD 2331−475.....	48514	L	1993 Aug 31	23399	150/77	−20.2	Vennes	Z
WD 2331−475.....	48522	L	1993 Sep 1	23700	151/94	−34.7	Vennes	Z
WD 2350−706.....	49030	L	1993 Oct 28	42292	209/145	...	Sion	Z
			He-rich Degenerates					
WD 0005+511.....	26191	L	1985 Jun 17	25200	206/111	−5.3	Sion	Z
WD 0005+511.....	52108	L	1994 Sep 14	21600	157/97	+4.7	Holberg	Z
WD 0005+511.....	52146	L	1994 Sep 17	25500	178/106	+5.9	Holberg	Z
WD 0005+511.....	52185	L	1994 Sep 22	25500	171/107	−4.8	Holberg	Z
WD 0044−121.....	3353	L	1978 Nov 15	6720	170/53	−42.4	Heap	Z
WD 0044−121.....	41997	L	1991 Jul 3	7200	156/40	−3.2	Cassatella	Z
WD 0044−121.....	42068	L	1991 Jul 13	13380	224/59	−5.1	Heap	Z
WD 0044−121.....	42073	L	1991 Jul 15	6900	150/39	+10.2	Tweedy	Z
WD 0044−121.....	42104	L	1991 Jul 20	9000	181/48	−6.5	Demartino	Z
WD 0044−121.....	42214	L	1991 Aug 10	9000	179/48	−5.3	Talavera	Z
WD 0044−121.....	42247	L	1991 Aug 14	7200	154/48	+39.5	Monier	Z
WD 0044−121.....	47843	L	1993 Jun 10	9896	216/76	−5.3	Quigley	Z
WD 0044−121.....	47844	L	1993 Jun 10	8097	186/84	+17.7	Quigley	Z
WD 0112+104.....	37656	L	1989 Nov 22	48000	180/109	0.0	Sion	W
WD 0501−289.....	46428	L	1992 Dec 7	28499	152/98	+3.1	Sion	Z
WD 0501−289.....	49788	L	1994 Jan 7	21896	133/90	+7.5	Holberg	Z
WD 0501−289.....	52796	L	1994 Nov 13	49499	235/163	−17.8	Holberg	Z
WD 0501−289.....	52803	L	1994 Nov 14	36299	190/129	−40.7	Holberg	Z
WD 1034+001.....	18509	L	1982 Nov 8	19800	195/70	−5.3	Sion	Z
WD 1034+001.....	26201	L	1985 Jun 18	15719	149/58	+5.3	Sion	Z
WD 1159−034.....	23032	L	1984 May 16	61199	230/164	+9.3	Liebert	Z
WD 1159−034.....	53903	L	1995 Feb 13	40015	226/171	−8.2	Holberg	Z
WD 1159−034.....	54675	L	1995 May 14	52499	231/164	−7.4	Burleigh	Z
WD 1159−034.....	54976	L	1995 Jun 10	52799	232/172	+2.4	Barstow	Z
WD 1211+332.....	31287	L	1987 Jul 3	68819	255/201	0.0	Sion	Z
WD 1634−573.....	6272	L	1979 Aug 24	5400	141/42	−24.0	Sion	Z
WD 1634−573.....	13781	L	1981 Apr 22	2400	205/148	−3.4	Raymond	Z
WD 1634−573.....	13782	L	1981 Apr 22	1680	119/83	+8.2	Raymond	Z
WD 1634−573.....	13783	L	1981 Apr 23	5340	140/81	+14.1	Raymond	Z
WD 1634−573.....	17467	L	1982 Jul 23	4500	159/92	+11.9	Bruhweiler	Z
WD 1645+325.....	31432	L	1987 Jul 29	63239	247/187	+27.2	Sion	Z
WD 1645+325.....	33681	L	1988 May 31	47700	207/155	−27.2	Sion	Z
WD 1821+643.....	33849	L	1988 Jul 1	47700	207/153	0.0	Holberg	Z
WD 2117+342.....	47556	L	1993 Apr 27	21600	168/87	+1.1	Levenhagen	Z
WD 2117+342.....	47563	L	1993 Apr 28	21720	172/61	−1.0	Leuenhagen	Z
WD 2117+342.....	55411	L	1995 Aug 3	26400	177/86	−39.8	Werner	Z

NEWSIPS versions of the data when they became available. This project presently includes 209 SWP spectra, the vast majority of which have useful signal levels. The NEWSIPS versions of all spectra have been processed with the exception of one spectrum, which could not be processed with NEWSIPS. A major effort has gone into the production of high-quality co-added spectra for the 33 stars, where suitable multiple spectra exist. This co-addition

procedure results in significant enhancements to the *IUE* data and has yielded a number of previously unsuspected discoveries from the *IUE* archives.

In Table 1 we list, according to WD number (McCook & Sion 1999), 55 degenerate objects with existing SWP echelle spectra. Included for each star is a commonly used alternate name, a spectral type from McCook & Sion, a visual magnitude, and an estimate of the effective temperature and surface gravity. The $T_{\rm eff}$ and log g determinations are of considerable theoretical importance in discussions of the photospheric abundances of heavy metals, and so we have provided references for these quantities. We have divided Table 1 into separate sections for the H-rich DA and DAO stars and the He-rich objects. This is done primarily because the He-rich objects tend to be much more luminous and distant and exhibit a richer variety of spectra than the DA stars. Although, for completeness, all 55 objects are listed, four targets have spectra that are too poorly exposed to be of any use. These are, WD 0134+833, WD 0343−007, WD 0518−105, and WD 0112+104. While the spectra of these stars are listed in Tables 1 and 2, no meaningful analysis of these four objects is possible. In addition to these stars, WD 2117+539 and WD 0612+177 possess useful signal levels but no stellar or interstellar lines could be identified in their spectra.

In Table 2 we present a log of all 209 SWP echelle spectra. Each spectrum is listed in order of WD number and SWP sequence number. The third column gives the SWP aperture, large (L) or small (S), through which the image was obtained. The calendar date of each exposure and the exposure length in seconds are given in the fourth and fifth columns, respectively. The continuum and background data number (DN) levels for each exposure are contained in the sixth column. For stars with multiple observations, the seventh column provides the wavelength shift in mÅ used to co-add the spectra. The definition of this shift is given in § 3.2. No shifts are applied to single spectra. The observer, as recorded in the spectral header, and the reduction and processing status are given in the final two columns. A status of "Z" indicates a fully processed NEWSIPS spectrum. "NS" indicates a low, unusable signal level, "B" indicates gross problems with the extracted spectrum, and 145S indicates only sky background owing to the star being partially or completely out of the aperture.

3. DATA REDUCTION AND MEASUREMENT

3.1. *Reduction of NEWSIPS Echelle Spectra*

NEWSIPS "MXHI" versions of all (except for SWP 40123) of the set of SWP spectra were obtained from the *IUE* Data Analysis Center (IUEDAC) and processed to a uniform standard. The data were processed using a set of specially designed IDL procedures. These procedures include the extraction of orders 71–121 using the current version of the READMX procedure. The resulting concatenated spectra were truncated to a wavelength range of 1150–1950 Å and then interpolated onto a standard, uniformly sampled, wavelength scale. At a sample step size of 0.03125 Å, this wavelength sampling preserves the original NEWSIPS sampling in the highest echelle orders but oversamples in the lowest orders. The absolutely scaled flux uncertainty vector was also extracted. The standard NEWSIPS data quality flag vector was mapped into a redefined flag vector which ranges between 1.0 (good data) and 0.001 (bad data), where any of the following conditions resulted in the flagging of a data point as "bad:" cosmic rays and bright spots, saturated pixels, permanent ITF artifacts, reseau marks in the ITF, uncalibrated data, and warning track. In addition to the above data flagging, positive noise spikes more than 4 σ in height were interpolated over and flagged as bad. Few negative noise spikes were deleted to avoid removing possible real absorption features. Finally, the raw spectra were digitally filtered with a low-pass filter having a cutoff at 50% in the frequency domain, rather than the three-point smoothing commonly used with IUESIPS data. After these processing steps, the spectra were saved for subsequent analysis as IDL save files. The absolute flux vectors are essentially those given by READMX, and no normalization or adjustments based on external data are made. Corrections to the NEWSIPS wavelength scale and the flux uncertainty vector, described respectively in §§ 3.4 and 3.5, were applied.

3.2. *Co-addition of Spectra*

If only a single useful spectrum of a star existed, no further processing was performed. For stars with more than one useful spectrum, the spectra were co-added to improve S/N. This procedure involved using narrow stellar and interstellar features to mutually register the spectra. A set of these features was carefully measured in each spectrum and the wavelength centroids for these features compared. A single constant wavelength shift was determined for each spectrum under the assumption that the observed wavelength shifts among the spectra are due to small differences in the placement of the stellar image within the SWP large aperture. The determination of these wavelength shifts depends on the number and strength of the features in each spectrum but in general is accurate to 10 mÅ or better. Registering the spectra in this fashion does not uniquely determine the velocity zero point of the resulting co-added spectrum. However, experience involving stars with independently known velocities indicates that this procedure yields absolute velocities accurate to 3–5 km s^{-1} During the co-addition procedure the spectra are shifted, resampled, and co-added onto the standard wavelength scale. The data points for each spectrum are weighted by the inverse square of the flux uncertainty vector during co-addition and bad data points are excluded. The general expression used to define a common wavelength (λ) scale is

$$\lambda_{\rm coadd} = \lambda_{\rm obs}\left(1 - \frac{v}{c}\right) + \Delta\lambda_{\rm shift}\,, \qquad (1)$$

where $\Delta\lambda_{\rm shift}$ and v are, respectively, the wavelength shift and Doppler velocity of each spectrum. Because NEWSIPS spectra are corrected to the heliocentric frame, Doppler velocities should be relevant only to binary stars. For binary stars with a known ephemeris such as Feige 24 and Feige 55, individual Doppler shifts can be applied to each spectrum, allowing co-addition in the stellar rest frame as well as the inertial frame. In these cases, both types of co-addition were performed. The final data quality flag is the simple mean of the flags, so that the value between 0.001 and 1 indicates the proportion of good and bad data contributing to each flux point.

3.3. *Measurement of Features*

All absorption features discussed herein were measured interactively by using a cursor to define the extremes of the

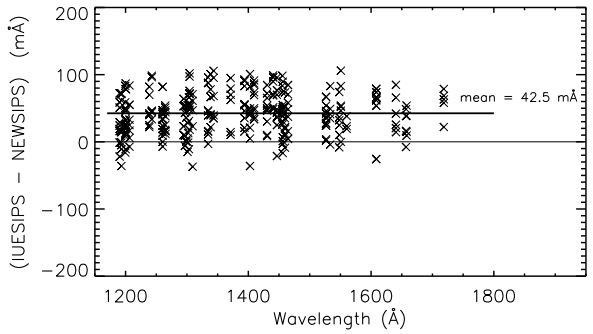

FIG. 1.—Apparent difference in wavelength scales between IUESIPS data and NEWSIPS data as a function of wavelength for the centroids of 320 lines in 38 spectra. The mean of the difference between the two scales is 42.5 mÅ.

wings of the line. The line parameters corresponding to the wavelength centroid and the equivalent width were determined with respect to a linear continuum drawn between the cursor locations. These quantities were determined in two ways: first, the wavelength centroid and equivalent width were calculated directly from the observed line profile; second, they were independently determined from Gaussian fits to the line. The associated uncertainties in the line parameters were simultaneously calculated using an inverse square weighting of the flux uncertainty vector. For features composed of more than one blended component, the measurements were made using fits to a multiple component Gaussian.

3.4. *Modification of Wavelength Scale*

During the initial analysis of the NEWSIPS data it was evident that the wavelengths of features were systematically different from the same features measured from IUESIPS data. In Figure 1, we illustrate this wavelength difference (IUESIPS − NEWSIPS) as a function of wavelength for 320 of the same features measured in some 38 spectra covering most of the life span of *IUE*. The mean wavelength offset for these lines is found to be 42.5 mÅ with a standard deviation of 30.4 mÅ. There is no discernible wavelength dependence to this offset. As a function of time, however, significant changes in the wavelength differences are apparent. In Figure 2 the average wavelength shift (IUESIPS − NEWSIPS) for each of 38 spectra are plotted, as a function of observation date. The large changes, most

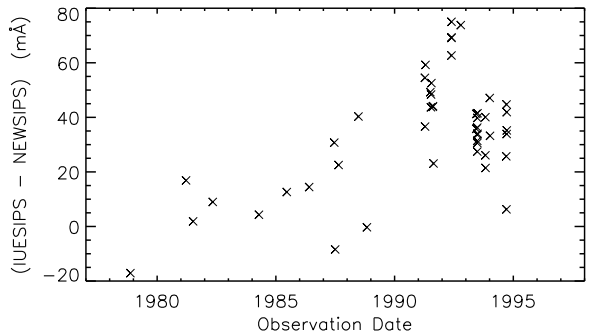

FIG. 2.—Apparent difference in wavelength scales between IUESIPS data and NEWSIPS data as a function of time. The mean wavelength difference (IUESIPS − NEWSIPS) for 38 spectra plotted as a function of observation date.

evident after 1992, are largely the result of modifications to the SWP dispersion coefficients instituted at that time (Garhart 1993). We have verified, however, that the wavelength differences do not result from our reduction of the NEWSIPS data. A more detailed study of the wavelength scales for both the SWP and LWP cameras and both apertures has been conducted by Smith (1998), who finds similar results.

Although we have adopted the NEWSIPS wavelength scale because it has been uniformly applied to the entire *IUE* archive, we must independently consider the zero point of the NEWSIPS velocity scale. Prior work with IUESIPS data generally showed good agreement with white dwarf radial velocities measured from Balmer profiles. For example, a weighted mean difference between ground-based and IUESIPS velocities for four stars is $+1.26 \pm 1.2$ km s^{-1}. These stars, Wolf 1346 (Holberg et al. 1996), EG 102 (Holberg, Barstow, & Green 1997, hereafter HBG), GD 394 (Barstow et al. 1996), and G191-B2B (Holberg et al. 1994), all have well-determined ground-based radial velocities obtained from their Balmer profiles and photospheric heavy element concentrations that allow *IUE* radial velocities to be determined. The ground-based − NEWSIPS velocity differences for these four stars have a weighted mean of $+8.30 \pm 1.4$ km s^{-1}. This latter difference is also consistent with ISM velocities measured by Lemoine et al. (1996) in the GHRS spectrum of the white dwarf G191-B2B. These authors find that the dominant and subordinate ISM velocity components for G191-B2B are located at $+9.9$ km s^{-1} and $+20.6$ km s^{-1} along the G191-B2B sight line. At *IUE* resolution, this would correspond to a blended line at $+13.7$ km s^{-1}, while the unresolved ISM lines in our NEWSIPS spectra of G191-B2B are at $+5.5 \pm 2.8$ km s^{-1}; this is a difference of $+8.2$ km s^{-1}. We have therefore applied a negative Doppler correction of 8.3 km s^{-1} to all of our NEWSIPS spectra.

3.5. *Modification of Uncertainty Vector*

During the course of working with the NEWSIPS data it was also noted that the standard flux uncertainty vectors produced by the READMX procedure appeared to be too large. The NEWSIPS uncertainty consistently produced wavelength and equivalent width uncertainties which were up to a factor of 2—3 larger than actually observed. We have, therefore, reduced the NEWSIPS uncertainty vector by a factor of 1.5, so that it can be used with standard error propagation formulas to produce more realistic uncertainties in the parameters of the line profiles.

In Figure 3 we plot an example of the increase in S/N as a function of the number of co-added NEWSIPS spectra. We have used a sequence of spectra of CD $-38°10980$, all with signal levels 100–120 DN above background and similar exposure times. The observed S/N is calculated for two continuum regions (1270–1290 Å and 1500–1520 Å) that are free of any stellar or interstellar features. For comparison, we also show an $n^{-1/2}$ increase in S/N expected for Poisson statistics from the combination of n spectra. We also show an identical S/N determination using the same spectra but with IUESIPS processing. As is evident, co-addition of NEWSIPS spectra does not fully realize optimal S/N gain but does continue to improve as more spectra are added. We have accounted for this increase in effective S/N in computing the co-added uncertainty vector. As a practical matter, however, more than six or seven spectra are

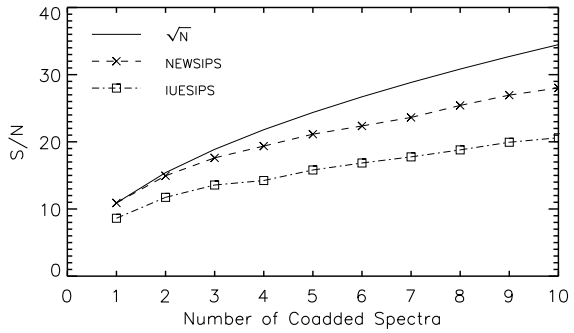

FIG. 3.—Relative increase in S/N for co-added spectra. The dashed curve represents the S/N in the 1500–1520 Å region of a series of co-added NEWSIPS spectra of CD −38°10980 as a function of the number of co-added spectra. The upper solid curve is a theoretical $n^{1/2}$ increase, where n is the number of co-added spectra. The solid curve has been normalized to the S/N of the first spectrum. The lower dashed-dot curve is the same as above except for IUESIPS spectra. In each case the same spectra have been co-added in the same order.

seldom co-added. The improvement in S/N afforded by NEWSIPS data over IUESIPS is also evident from this figure. The plot in Figure 3 is representative of this improvement at long wavelengths, and even greater gains are often seen in the 1150–1200 Å range.

4. IDENTIFICATION OF FEATURES

The identification of "features" in *IUE* echelle spectra is frequently more of an art than a science. For faint stars, such as white dwarfs, the S/N can be frustratingly low, sometimes only 2 or 3. Moreover, the detected flux is subject to fluctuations that cannot be as easily characterized as with count rate data. Large positive and negative "noise" spikes are frequently present as are "fixed pattern noise" features, cosmic-ray hits, camera reseau marks, and residual uncorrected echelle ripple. In the face of these difficulties, it is helpful that most white dwarf spectra are intrinsically simple, i.e., predominantly smooth photospheric continua. There may or may not be detectable features due to photospheric or circumstellar absorption lines, but there are nearly always at least a few features due to the ISM. Leaving aside for a moment such metal-rich stars such as G191-B2B, REJ 0623−374, and REJ 2214−491, the number of photospheric lines expected and observed in most white dwarfs is small, perhaps only a dozen or so. Likewise, the number of ISM lines is comparable. This substantially narrows the search for real features. When combined with arguments based on a common velocity system for each component, a reasonable range of ionization states, and a consideration of expected line strengths, the choice of features that need be considered is quite limited.

Another factor that hampered early interpretations of observed narrow interstellar-like lines was determining whether these features arose in the stellar photosphere, a circumstellar environment, or the ISM. In the absence of independent accurate and reliable measurements of the apparent stellar velocity, for example the Doppler shift of the Balmer lines, it is often difficult to know for certain the origin of a particular line. For example, an observed Si II 1260 Å line could arise in the stellar photosphere, the ISM, or elsewhere. Fortunately such decisions can often be successfully made from other information. For example, if the excited Si II lines at 1264, 1265, 1309, or 1533 Å are present and if they consistently yield a unique photospheric abundance they are presumed to be of photospheric origin as in the case of Wolf 1346 (Holberg et al. 1996). Alternately, if a consistent abundance is not found or if the observed velocity is not that of the photosphere, a circumstellar origin is implied, as with CD −38°10980 (VTS; Holberg, Bruhweiler, & Andersen 1995a, hereafter HBA).

4.1. *Photospheric Features*

Many white dwarfs show narrow absorption lines indicating the presence of elements heavier than hydrogen and helium in their photospheres. A summary of the ions and examples of some of the lines that have been detected, predominantly with *IUE*, in the spectra hot white dwarfs is given in Table 3. Also included are examples of some of the more prominent stars in which these features have been observed. The thin photospheres of white dwarfs have highly nonsolar chemical abundances, which reflects both the strong gravitational field and poorly understood processes occurring in their pre–white dwarf stages of evolution. The observed patterns of heavy element abundance offer some of the most important clues we have as to the physical processes that shape the photospheric chemical composition of these stars. Perhaps the most striking pattern is the abrupt change in heavy element content exhibited by the DA white dwarfs as they cool from above 55,000 K to below 50,000 K (Marsh et al. 1997 and others). This pattern was first apparent from systematic EUV observations (Barstow et al. 1993), where the average levels of EUV opacity were seen to decrease dramatically over this temperature range to the low levels characteristic of pure hydrogen photospheres. It is now clear (Tweedy 1993; Holberg et al. 1993) that these high levels of EUV opacity are associated with high heavy element abundance, in particular Fe and Ni, which are evident as a host of UV absorption lines occurring chiefly in the wavelength region of the SWP camera. An example of such a star is the hot DA star REJ 2214−491. In Figure 4 we show the 1320–1340 Å region of our co-added spectrum of REJ 2214−491, which contains numerous Fe V and Ni V lines. It has proved essential to have independent estimates of such abundances from *IUE* and now *HST* to model adequately the EUV spectra of these hot metal-rich stars (Lanz et al. 1996). Current efforts at refining such model atmospheres (Barstow, Hubeny, & Holberg 1998; Wolff et al. 1998) indicate that there exist metal abundance hierarchies among the very hottest DA white dwarfs.

The abrupt change in photospheric content of DA stars near 55,000 K is consistent with the predictions of radiative levitation (Chayer, Fontaine, & Wesemael 1995), where heavy elements are most effectively levitated by radiation pressure above this temperature. Beyond this qualitative agreement, however, the detailed abundance predictions encounter considerable difficulty. Radiative levitation is fundamentally an equilibrium process in which effective temperature and gravity determine the photospheric concentration of a given ion, provided there exists a sufficient internal or external reservoir of the element. The abundances of a few ions in the observed spectra of a few stars appear to agree with the equilibrium predictions, but most do not (Chayer et al. 1995; Holberg et al. 1997). For example, while the silicon abundance in the 20,000 K DA Wolf 1346 (Holberg et al. 1996) agrees with predictions, the

TABLE 3

PHOTOSPHERIC FEATURES DETECTED IN HOT H-RICH WHITE DWARFS

Ion	Lines (Å)	Example(s)	Instrument	References
C III	λλ1176	G191-B2B	*IUE*, *HST*	1, 2
C IV	1548, 1550	G191-B2B	*IUE*	3
N IV	1718	G191-B2B	*IUE*	4
N V	1238, 1242	G191-B2B	*IUE*	3
O IV	1338, 1343	RE 2214−492	*IUE*	5
O V	1371	RE 2214−492	*IUE*	5
Mg II	4481	EG 102	Ground	6
Al II	1670	EG 102	*IUE*	7
Al III.....	1854, 1862	RE 2214−492, GD 394	*IUE*	4, 7
Si II	1264, 1265	Wolf 1346	*IUE*	8
Si III	λλ1296	GD 394	*IUE*	8
Si IV	1393, 1402	G191-B2B,GD 394	*IUE*	3, 8
P V	1117, 1128	G191-B2B	ORFEUS	9
S IV	1062, 1072	G191-B2B	ORFEUS	9
Ca II	3933	EG 102	Ground	10
Fe V	Numerous	G191-B2B	*HST*	2
Fe VI	Numerous	G191-B2B	*IUE*	5
Fe VII.....	1239, 1244	S 216	*IUE*	11, 12
Ni V	Numerous	G191-B2B	*IUE*	13

REFERENCES.—(1) Holberg 1995; (2) Sion et al. 1992; (3) Bruhweiler & Kondo 1981; (4) Holberg et al. 1993; (5) Tweedy 1991; (6) HBG; (7) this paper; (8) Bruhweiler & Kondo 1983; (9) Vennes et al. 1996; (10) Zuckerman & Reid 1998; (11) Tweedy & Napiwotzki 1992; (12) Feibelman & Bruhweiler 1990; (13) Holberg et al. 1994.

36,000 DA star GD 394 (see Fig. 5) is observed to possess a superabundance of silicon (Barstow et al. 1996). Additionally, many other stars have silicon abundances orders of magnitude below predicted levels (HBG). These wide departures of observed abundances, both over and above predicted abundances, are a clear indication that processes other than gravity and diffusion are important in determining the composition and structure of white dwarf photospheres. Accretion of heavy elements from circumstellar material or the ISM and the expelling of heavy elements through mass loss and weak winds are examples of such nonequilibrium processes. Convincing examples of ongoing accretion among hot white dwarfs are limited. The 20,000 K DA star EG 102 is known from optical and *IUE* spectra to have extremely high levels of the refractory elements magnesium and aluminum (HBG). The photospheric residence times for such ions is only a few days and the implication is that these species are almost certainly the result of ongoing accretion. Other examples exist in cooler DAZ stars such as G29-38 (12,000 K), where Ca, Mg, and Fe features (Zuckerman & Reid 1998) are observed and in the DBZ star GD 40 (15,000 K), where a host of features due to Ca, Mg, and Fe are observed (Shipman 1984). Although these may also represent instances of accretion and may be linked to the DBA

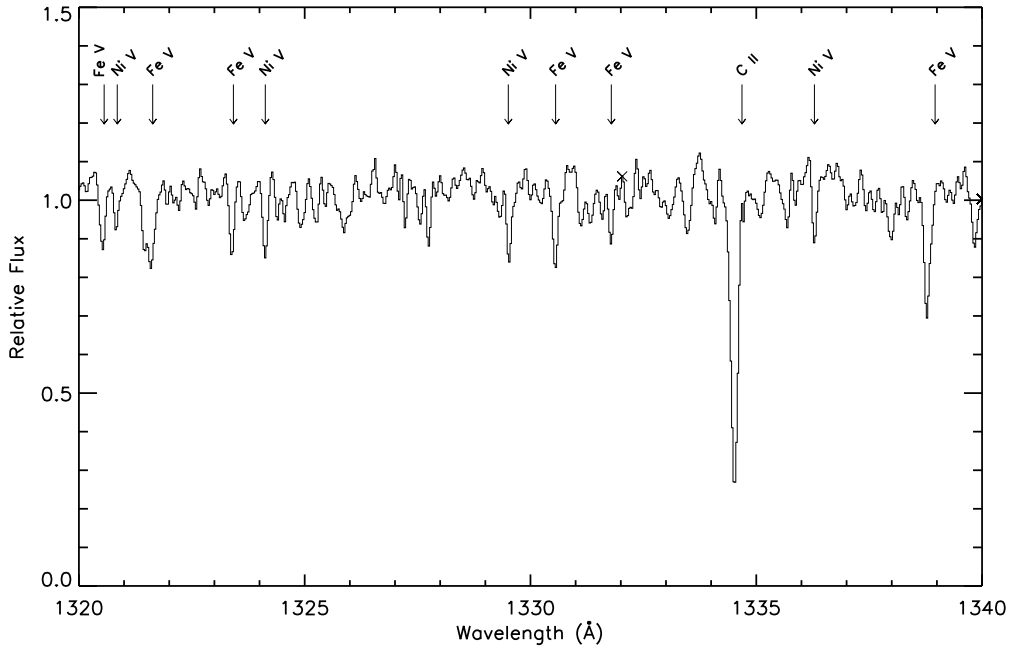

FIG. 4.—Co-added NEWSIPS spectrum showing the 1320–1340 Å region of the metal-rich hot DA star REJ 2214−491. The arrows indicate the presence of photospheric lines due to Fe V and Ni V, as well as interstellar C II.

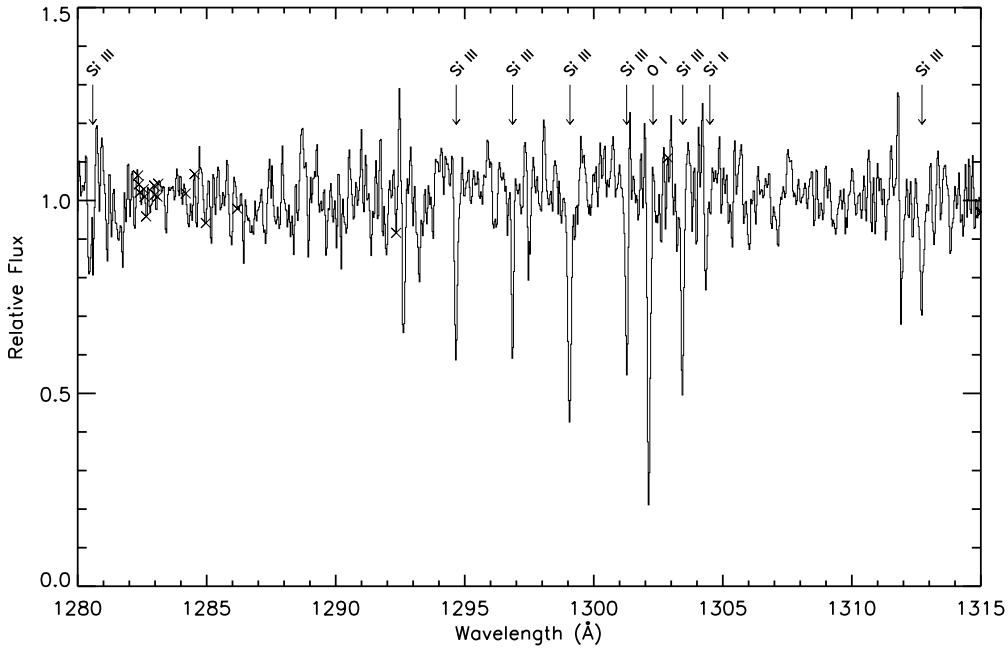

FIG. 5.—Co-added spectrum showing the 1280–1315 Å region of the Si-rich hot DA star GD 394. The arrows indicate the presence of photospheric lines due to highly excited Si III, as well as interstellar O I and Si II.

phenomena, the residence times for heavy elements in the photospheres of these cooler stars is much longer than that of EG 102. Examples of the opposite and more widespread process of mass loss are discussed in the next section.

In Table 4 we list, by star, the photospheric lines from elements heavier than hydrogen. For each line we list the laboratory wavelength taken from Morton (1991), Kelly & Palumbo (1973), Wiese, Smith, & Glennon (1966), or elsewhere, the observed wavelength, and the corresponding Doppler velocity and uncertainty. Also listed are the measured equivalent widths and uncertainties for each line. The list of photospheric lines in Table 4 is not intended to be exhaustive. We have included only those lines that we are relatively certain are real; in general, we have adopted a 2 σ detection limit. Also many elements have no strong lines in the SWP spectral region. For example, P V and S IV lines were observed in the ORFEUS spectra of two DA stars below 1200 Å (Vennes et al. 1996), but these elements have no lines observable in *IUE* spectra. Finally, for very metal-rich stars such as G191-B2B we list only the dozen or so of the most prominent of the many Fe and Ni lines. Further work on the photospheric features, including abundance estimates, will be presented elsewhere.

4.1.1. *Circumstellar Features*

Nonphotospheric features, due either to mass loss or circumstellar gas, are important as they offer key evidence for nonequilibrium processes that can dramatically modify the chemical composition of white dwarf photospheres. In DA stars such evidence is relatively scarce, but good examples do exist. Circumstellar features, of a very different nature, have been previously reported in at least two DA white dwarfs: CD $-38°10980$ and GD 659. In CD $-38°10980$, HBA have shown that there exists a set of excited C II, Si II, Si III lines, and weak C IV resonance lines with a radial velocity $+12.1 \pm 2.1$ km with respect to the stellar photosphere. These authors also demonstrated that these lines are primarily photoexcited. The velocity difference and nature of the excitations led the authors to propose a dense photoexcited region very near the star. It is not known how such a circumstellar zone is formed near a white dwarf nor why CD $-38°10980$ is unique so far in having such a zone. In GD 659, Holberg et al. (1995a) examined the peculiar set of high excitation lines (see Fig. 6) due to N V, C IV, and Si IV, first noted by VTS, and showed that these lines do not arise in the stellar photosphere and were unlikely to be interstellar lines unrelated to the star. There is a very large redshift difference of 72 km s^{-1} between the velocity of the lines and the reported velocity of the stellar photosphere. Holberg et al. (1995a) suggest that these lines are formed in a highly ionized circumstellar or interstellar region some distance from the star.

In general, DA stars are devoid of blueshifted components of the major resonance lines. However, there now exist two important examples of such features indicating the presence of ongoing mass loss. Holberg et al. (1997) observed the 36,000 K DA, REJ 1614−085, with the GHRS and found a very high, nonequilibrium abundance of nitrogen and evidence of weak blueshifted features in the Si IV and C IV resonance lines. The metal-rich hot DA REJ 0457−281 also shows (Holberg et al. 1998b) evidence of weak blueshifted features in the C IV and Si IV lines (see Fig. 7) in addition to photospheric lines of these ions. In Table 5 we list the circumstellar and blueshifted features found in our *IUE* spectra. In this paper we regard any nonphotospheric C IV, Si IV, or N V resonance lines as circumstellar and not interstellar. There are a number of aspects that distinguish such features from interstellar lines. Among the most important are the almost total lack of any examples of such features within the local ISM and the rather large column densities of these highly ionized species implied by the lines seen in the white dwarf spectra. Another distinguishing characteristic is the rather narrow range of blue shifts (40–60 km s^{-1}) of the circumstellar lines when ISM lines exhibit both red- and blueshifts with respect to the stellar photospheres. These and other characteristics of

TABLE 4

PHOTOSPHERIC LINES

WD Number/ Species	Lab. (λ) Å	Obs. (λ) Å	V (km s^{-1})	σ (km s^{-1})	EW (mÅ)	σ (mÅ)
		H-rich Degenerates				
WD 0232+035:						
N v	1238.8210	1239.0996	67.41	1.98	68	5
N v	1242.8040	1243.0668	63.90	2.56	53	6
N iv	1718.5510	1718.9971	77.81	2.90	21	5
Si iv	1393.7550	1394.0952	73.18	2.16	77	7
Si iv	1402.7770	1403.0927	67.46	1.96	71	6
C iv.....	1548.2020	1548.5599	69.31	1.47	65	6
C iv.....	1550.7740	1551.1464	71.97	1.71	79	7
O iv	1338.6121	1338.9568	77.20	4.32	17	5
O iv	1343.5120	1343.8632	78.37	4.26	19	6
O v	1371.2920	1371.5747	61.81	4.80	18	5
Fe v	1387.9370	1388.2371	64.81	5.38	14	5
Fe v	1402.3850	1402.7238	72.42	2.07	28	5
Fe v	1407.2460	1407.5898	73.26	6.01	13	6
Fe v	1409.2200	1409.5510	70.43	4.71	14	6
Fe v	1409.4510	1409.7812	70.23	4.89	17	6
Fe v	1430.5730	1430.8848	65.33	4.58	20	6
Fe v	1440.5280	1440.8303	62.93	3.26	22	6
Fe v	1446.6169	1446.9551	70.07	5.06	18	6
Fe v	1448.8459	1449.2068	74.66	6.29	14	6
Fe v	1455.5590	1455.8884	67.86	5.42	27	8
Fe v	1456.1620	1456.5443	78.71	4.76	36	9
Fe v	1459.8280	1460.1624	68.66	3.71	24	7
Fe v	1464.6860	1465.0343	71.28	3.64	22	6
Ni v	1250.3879	1250.6600	65.24	5.05	14	5
Ni v	1264.5010	1264.8062	72.35	3.34	14	4
Ni v	1266.4080	1266.7017	69.53	8.93	10	6
Ni v	1336.1360	1336.4811	77.43	7.87	11	5
		$\langle V \rangle$	+70.13	0.58		
WD 0441+467:						
He ii	1640.5050	1640.5822	14.10	1.75	92	12
N v	1238.8210	1238.8585	9.07	2.03	213	9
N v	1242.8040	1242.8656	14.87	2.45	203	12
N iv	1718.5510	1718.6562	18.36	7.60	42	10
Si iv	1393.7550	1393.7954	8.69	2.05	80	9
Si iv	1402.7770	1402.8124	7.57	3.12	55	9
C iv.....	1548.2020	1548.2548	10.21	1.91	216	14
C iv.....	1550.7740	1550.8344	11.66	1.82	177	13
O iv	1338.6121	1338.6847	16.27	3.84	56	7
O iv	1343.5120	1343.5540	9.37	3.57	79	11
O v	1371.2920	1371.3364	9.71	1.93	141	10
Fe vi	1227.8820	1227.9281	11.27	5.11	23	7
Fe vi	1252.7820	1252.8423	14.43	3.57	42	8
Fe vi	1272.0649	1272.1110	10.85	2.54	43	6
Fe vi	1278.2910	1278.3185	6.44	4.77	40	10
Fe vi	1287.0300	1287.0598	6.94	4.03	42	8
Fe vi	1370.7280	1370.7869	12.87	4.70	40	10
Fe vi	1374.6270	1374.6665	8.63	4.07	39	8
Fe vii	1239.6899	1239.7206	7.41	8.51	20	8
Fe vii	1244.4420	1244.4963	13.09	7.74	14	8
		$\langle V \rangle$	+11.01	0.62		
WD 0455−282:						
N v	1238.8210	1239.1021	68.00	3.82	44	10
N v	1242.8040	1243.0863	68.11	4.23	48	13
Si iv	1393.7550	1394.0762	69.08	4.27	54	14
Si iv	1402.7770	1403.1122	71.64	4.93	42	14
C iv.....	1548.2020	1548.5576	68.86	9.24	28	21
C iv.....	1550.7740	1551.1639	75.37	6.31	75	24
		$\langle V \rangle$	+69.60	1.97		
WD 0501+527:						
N v	1238.8210	1238.9039	20.06	2.50	70	6
N v	1242.8040	1242.8813	18.67	2.50	55	6
Si iv	1393.7550	1393.8704	24.81	1.52	76	5
Si iv	1402.7770	1402.8802	22.07	1.75	64	5
C iii.....	1174.9330	1175.0256	23.64	3.68	26	7
C iii.....	1176.3700	1176.4814	28.40	5.52	16	7
C iv.....	1548.2020	1548.3036	19.67	1.37	159	7
C iv.....	1550.7740	1550.8944	23.27	1.32	134	7
O iv	1338.6121	1338.6996	19.60	6.33	15	6
O iv	1343.5120	1343.6078	21.38	3.07	21	5
O v	1371.2920	1371.3654	16.04	6.14	14	5

TABLE 4—*Continued*

WD Number/ Species	Lab. (λ) Å	Obs. (λ) Å	V (km s^{-1})	σ (km s^{-1})	EW (mÅ)	σ (mÅ)
Al III	1854.7164	1854.8560	22.55	4.29	10	4
Al III	1862.7896	1862.8801	14.58	4.79	10	4
Fe V	1387.9370	1388.0411	22.49	3.28	20	5
Fe V	1409.2200	1409.3212	21.53	4.00	15	5
Fe V	1409.4510	1409.5276	16.28	4.48	22	6
Fe V	1430.5730	1430.6925	25.04	3.76	22	5
Fe V	1440.5280	1440.6542	26.27	3.26	26	6
Fe V	1446.6169	1446.7126	19.83	5.36	16	6
Fe V	1448.8459	1448.9369	18.82	4.57	10	5
Fe V	1455.5590	1455.6726	23.41	3.31	20	6
Fe V	1456.1620	1456.2844	25.21	3.09	17	6
Fe V	1459.8280	1459.9163	18.12	4.65	20	7
Fe V	1464.6860	1464.7819	19.61	3.17	30	6
Ni V	1250.3879	1250.4895	24.35	5.86	13	4
Ni V	1311.1060	1311.2067	23.03	4.86	14	5
Ni V	1336.1360	1336.2356	22.35	6.03	9	5
		$\langle V \rangle$	+21.98	0.54		
WD 0512+326:						
Si IV	1393.7550	1393.8657	23.82	4.06	85	21
Si IV	1402.7770	1402.8630	18.39	9.16	34	21
		$\langle V \rangle$	+22.92	3.71		
WD 0621−376:						
N V	1238.8210	1238.9816	38.85	2.05	110	7
N V	1242.8040	1242.9534	36.04	2.24	76	7
N IV	1718.5510	1718.8036	44.06	2.45	39	6
Si IV	1393.7550	1393.9452	40.91	1.88	89	7
Si IV	1402.7770	1402.9517	37.33	2.00	84	7
C IV	1548.2020	1548.3987	38.08	1.63	122	9
C IV	1550.7740	1551.0161	46.80	4.12	148	10
Al III	1854.7164	1854.9319	34.83	4.58	29	6
Al III	1862.7896	1863.0725	45.55	4.08	30	6
O IV	1338.6121	1338.8184	46.20	2.36	53	6
O IV	1343.5120	1343.7097	44.13	2.68	42	7
O V	1371.2920	1371.4476	34.03	2.38	45	6
Fe V	1376.3370	1376.5515	46.72	2.23	73	6
Fe V	1387.9370	1388.1292	41.50	3.71	33	7
Fe V	1402.3850	1402.5911	44.05	3.29	53	8
Fe V	1407.2460	1407.4265	38.46	4.65	35	8
Fe V	1409.2200	1409.4227	43.13	2.66	30	7
Fe V	1409.4510	1409.6464	41.54	2.96	41	7
Fe V	1430.5730	1430.7817	43.74	2.71	58	7
Fe V	1440.5280	1440.7070	37.27	3.25	32	7
Fe V	1446.6169	1446.7856	34.96	2.77	46	7
Fe V	1448.8459	1449.0361	39.35	2.74	34	7
Fe V	1455.5590	1455.7649	42.42	3.13	54	9
Fe V	1459.8280	1460.0231	40.06	2.21	56	8
Fe V	1464.6860	1464.8641	36.45	3.47	41	8
Fe V	1554.2150	1554.4510	45.54	7.04	18	10
Fe VI	1252.7820	1252.9333	36.22	6.29	19	7
Fe VI	1272.0649	1272.2166	35.73	3.60	21	5
Fe VI	1278.2910	1278.3969	24.82	8.76	15	8
Fe VI	1287.0300	1287.2289	46.32	3.33	24	5
Ni V	1250.3879	1250.5547	39.98	2.81	29	5
Ni V	1261.7600	1261.9103	35.70	3.32	23	5
Ni V	1264.5010	1264.6970	47.17	2.84	24	5
Ni V	1266.4080	1266.5835	41.55	6.60	19	7
Ni V	1311.1060	1311.2961	43.49	4.62	32	7
Ni V	1317.4470	1317.5991	34.61	5.06	25	7
Ni V	1323.9771	1324.1512	39.44	5.40	20	6
Ni V	1336.1360	1336.3367	45.03	4.74	29	6
		$\langle V \rangle$	+40.49	0.47		
WD 1148−230:						
He II	1640.5050	1640.2944	−38.48	5.26	427	36
N V	1238.8210	1238.7538	−16.28	2.48	234	19
N V	1242.8040	1242.7296	−17.93	4.42	189	27
N IV	1718.5510	1718.3710	−31.41	3.88	271	24
Si IV	1402.7770	1402.7209	−11.97	4.12	48	14
C IV	1548.2020	1548.1635	−7.47	5.80	173	30
C IV	1550.7740	1550.7888	2.86	4.80	175	27
		$\langle V \rangle$	−17.50	1.49		

TABLE 4—*Continued*

WD Number/ Species	Lab. (λ) Å	Obs. (λ) Å	V (km s^{-1})	σ (km s^{-1})	EW (mÅ)	σ (mÅ)
WD 1202+608:						
He II	1640.5050	1640.4071	−17.89	6.72	35	22
N V	1238.8210	1238.7870	−8.24	5.18	95	18
N V	1242.8040	1242.7947	−2.24	6.07	109	21
N IV	1718.5510	1718.5782	4.75	3.90	54	16
Si IV	1393.7550	1393.7637	1.86	3.60	68	16
Si IV	1402.7770	1402.7903	2.84	7.59	27	15
C IV.....	1548.2020	1548.1646	−7.26	6.02	74	25
C IV.....	1550.7740	1550.8472	14.14	7.20	90	21
O IV	1343.5120	1343.4542	−12.88	7.16	44	19
O V	1371.2920	1371.2632	−6.30	7.61	46	19
Fe V	1387.9370	1387.9133	−5.11	8.22	38	17
Fe V	1402.3850	1402.3767	−1.77	7.68	37	18
Fe V	1430.5730	1430.6179	9.41	6.12	30	16
Fe V	1446.6169	1446.5605	−11.69	7.31	34	19
Fe V	1448.8459	1448.8551	1.89	7.03	40	18
Fe V	1459.8280	1459.8497	4.46	6.29	47	22
Fe VI	1227.8820	1227.8711	−2.65	6.80	32	14
Fe VI	1252.7820	1252.7524	−7.07	6.80	31	14
Ni V	1264.5010	1264.5049	0.93	9.07	29	15
Ni V	1318.5150	1318.4851	−6.80	6.26	28	14
Ni V	1323.9771	1323.9670	−2.27	9.24	22	14
		$\langle V \rangle$	−1.59	1.35		
WD 1210+533:						
He II	1640.5050	1640.4225	−15.08	3.51	325	49
		$\langle V \rangle$	−15.08	3.51		
WD 1337+705:						
Si II	1260.4221	1260.4150	−1.68	3.67	93	21
Si II	1526.7065	1526.7477	8.08	9.55	44	29
Si II*.....	1264.7377	1264.7388	0.26	3.67	83	21
Si II*.....	1309.2758	1309.2498	−5.95	7.62	30	17
Si II*.....	1533.4312	1533.4193	−2.32	4.22	65	25
Al II.....	1670.7874	1670.7902	0.50	10.47	82	55
Al III	1854.7164	1854.7130	−0.40	2.29	148	19
Al III	1862.7896	1862.8086	3.07	4.38	70	24
		$\langle V \rangle$	−0.33	1.44		
WD 2032+248:						
Si II	1260.4221	1260.4999	18.49	4.00	46	14
Si II	1304.3702	1304.4967	29.07	5.09	19	23
Si II	1526.7065	1526.8638	30.87	4.20	31	26
Si II*.....	1264.7377	1264.8419	24.71	3.01	75	10
Si II*.....	1265.0020	1265.0831	19.24	3.30	51	9
Si II*.....	1309.2758	1309.3623	19.82	4.06	28	7
Si II*.....	1533.4312	1533.5496	23.15	3.20	48	9
Si III	1296.7260	1296.8229	22.41	8.09	15	7
Si III	1298.9510	1299.0369	19.81	5.24	27	8
		$\langle V \rangle$	+22.89	1.32		
WD 2111+498:						
Si III	1206.5220	1206.6473	31.15	5.89	99	26
Si III	1280.3540	1280.4680	26.70	6.95	35	16
Si III	1294.5430	1294.6744	30.45	3.43	65	11
Si III	1296.7260	1296.8550	29.83	2.57	45	9
Si III	1298.9510	1299.0619	25.58	2.59	90	11
Si III	1301.1460	1301.2651	27.45	2.91	64	11
Si III	1303.3199	1303.4370	26.93	3.04	66	13
Si III	1312.5900	1312.7164	28.88	4.80	49	12
Si III	1341.4650	1341.5769	25.02	5.67	28	13
Si III	1342.3920	1342.5442	33.99	3.70	54	13
Si III	1343.3879	1343.4935	23.56	4.59	30	13
Si III	1365.2531	1365.3961	31.42	4.44	31	11
Si III	1417.2371	1417.3690	27.91	4.19	64	16
Si III	1435.7720	1435.9167	30.23	4.73	47	16
Si III	1500.2410	1500.3877	29.32	3.52	81	19
Si III	1501.1910	1501.3339	28.52	3.21	33	14
Al III	1854.7159	1854.9083	31.10	2.67	68	12
Al III	1862.7900	1862.9580	27.03	5.07	76	17
Si IV	1393.7550	1393.9076	32.82	3.18	276	21
Si IV	1402.7770	1402.9037	27.08	3.44	168	19
		$\langle V \rangle$	+28.90	0.80		

TABLE 4—*Continued*

WD Number/ Species	Lab. (λ) Å	Obs. (λ) Å	V (km s^{-1})	σ (km s^{-1})	EW (mÅ)	σ (mÅ)
WD 2214−495:						
N v	1238.8210	1238.9370	28.06	2.60	113	5
N v	1242.8040	1242.9216	30.80	2.85	97	6
N iv	1718.5510	1718.7753	39.12	3.23	59	6
Si iv	1393.7550	1393.9055	32.38	1.58	77	6
Si iv	1402.7770	1402.9299	32.69	2.11	93	7
C iv.....	1548.2020	1548.3545	29.52	3.11	146	8
C iv.....	1550.7740	1550.9800	39.81	4.50	153	10
O iv	1338.6121	1338.7855	38.85	2.23	51	5
O iv	1343.5120	1343.6742	36.20	2.98	47	6
O v	1371.2920	1371.4214	28.29	1.78	54	5
Fe v	1376.3370	1376.5260	41.16	1.87	58	5
Fe v	1387.9370	1388.0988	34.94	2.70	37	5
Fe v	1402.3850	1402.5409	33.32	2.87	50	6
Fe v	1407.2460	1407.4088	34.69	3.99	24	6
Fe v	1409.2200	1409.3972	37.71	3.64	18	6
Fe v	1409.4510	1409.6206	36.06	2.08	38	6
Fe v	1430.5730	1430.7389	34.76	2.46	34	5
Fe v	1440.5280	1440.6884	33.38	2.81	31	6
Fe v	1446.6169	1446.7699	31.70	3.34	29	6
Fe v	1448.8459	1448.9977	31.40	2.86	27	6
Fe v	1455.5590	1455.7400	37.29	3.50	32	7
Fe v	1459.8280	1460.0165	38.71	2.83	47	7
Fe v	1464.6860	1464.8547	34.53	2.65	43	6
Fe vi	1252.7820	1252.9187	32.72	3.67	26	5
Fe vi	1272.0649	1272.1858	28.48	2.73	27	4
Fe vi	1287.0300	1287.1743	33.61	3.08	31	5
Fe vi	1370.7280	1370.8793	33.08	4.18	14	5
Ni v	1250.3879	1250.5234	32.49	2.96	34	5
Ni v	1261.7600	1261.8833	29.29	5.51	15	5
Ni v	1264.5010	1264.6526	35.94	3.64	21	5
Ni v	1266.4080	1266.5386	30.92	5.46	16	6
Ni v	1311.1060	1311.2393	30.48	2.94	19	4
Ni v	1317.4470	1317.6064	36.28	4.60	24	6
Ni v	1323.9771	1324.1259	33.69	3.31	22	5
Ni v	1336.1360	1336.2971	36.15	3.20	20	4
Ni v	1353.1121	1353.2676	34.46	4.39	10	4
		$\langle V \rangle$	+33.91	0.47		
WD 2309+105:						
Si iv	1393.7550	1393.6938	−13.15	2.65	54	8
Si iv	1402.7770	1402.7164	−12.94	4.12	51	10
C iv.....	1548.2020	1548.1499	−10.09	4.47	64	14
C iv.....	1550.7740	1550.7052	−13.31	2.04	67	10
		$\langle V \rangle$	−12.89	1.43		
WD 2331−475:						
N v	1238.8210	1238.9648	34.80	7.52	27	11
N v	1242.8040	1242.8934	21.58	7.29	33	14
Si iv	1393.7550	1393.9576	43.59	3.74	84	15
Si iv	1402.7770	1402.9585	38.79	3.84	66	13
C iv.....	1548.2020	1548.4707	52.03	8.06	17	15
C iv.....	1550.7740	1550.9779	39.41	4.39	41	17
		$\langle V \rangle$	+39.55	2.03		
		He-rich Degenerates				
WD 0005+511:						
N v	1238.8210	1238.9506	38.87	2.21	40	9
N v	1242.8040	1242.9651	31.34	2.94	31	8
C iv.....	1230.5210	1230.6692	36.10	10.14	25	15
		$\langle V \rangle$	+36.15	1.74		
WD 0044−121:						
O v	1371.2920	1371.1949	−21.22	2.57	47	5
C iv.....	1168.8470	1168.7679	−20.29	5.10	80	15
C iv.....	1230.5210	1230.4349	−20.97	2.29	59	5
C iv.....	1315.6250	1315.5240	−23.00	2.19	49	5
C iv.....	1351.2159	1351.1005	−25.62	2.96	67	4
C iv.....	1440.2830	1440.2094	−15.32	5.30	31	5
		$\langle V \rangle$	−22.00	1.16		
WD 0501−289:						
N v	1238.8210	1238.9659	35.06	3.54	156	14
N v	1242.8040	1242.9343	31.45	3.70	107	15

TABLE 4—*Continued*

WD Number/ Species	Lab. (λ) Å	Obs. (λ) Å	V (km s^{-1})	σ (km s^{-1})	EW (mÅ)	σ (mÅ)
N IV	1718.5510	1718.7863	41.03	3.31	112	17
Si IV	1393.7550	1393.9397	39.73	4.28	56	15
Si IV	1402.7770	1402.9479	36.82	3.18	46	14
C IV.....	1548.2020	1548.3602	30.63	6.64	239	44
C IV.....	1550.7740	1550.9839	40.57	5.75	208	42
O IV	1338.6121	1338.8019	42.51	2.34	64	10
O IV	1343.5120	1343.7189	46.17	6.16	53	17
O V	1371.2920	1371.4882	42.89	4.34	91	15
C III.....	1174.9330	1175.1040	43.64	15.34	58	42
C III.....	1175.5900	1175.7709	46.13	9.27	64	40
C III.....	1175.7111	1175.8853	44.44	9.27	22	13
C III.....	1175.9871	1176.1815	49.57	17.34	55	49
C III.....	1176.3700	1176.5850	54.78	15.25	62	48
C III.....	1247.3831	1247.5405	37.85	4.47	65	13
		$\langle V \rangle$	+39.32	1.12		
WD 1034+001:						
He II.....	1640.5050	1640.7910	52.27	6.31	45	10
N V	1238.8210	1239.0165	47.29	3.35	130	14
N V	1242.8040	1243.0144	50.76	4.77	147	18
Si IV	1393.7550	1394.0065	54.09	4.94	39	12
Si IV	1402.7770	1403.0704	62.72	6.49	30	12
C IV.....	1548.2020	1548.4723	52.33	6.52	31	16
C IV.....	1550.7740	1551.0593	55.15	4.46	59	16
O V	1371.2920	1371.5106	47.80	3.12	83	12
Fe VI	1252.7820	1252.9880	49.31	6.58	21	10
Fe VI	1272.0649	1272.2880	52.56	6.61	30	9
Fe VI	1278.2910	1278.5238	54.60	9.83	22	12
Fe VI	1370.7280	1370.9543	49.50	5.14	14	9
Fe VI	1374.6270	1374.8372	45.84	5.01	35	11
Fe VII.....	1226.6530	1226.8693	52.87	10.29	25	13
Fe VII.....	1332.3810	1332.6268	55.32	6.30	29	11
		$\langle V \rangle$	+50.83	1.33		
WD 1159−034:						
N V	1238.8210	1239.0188	47.86	4.55	127	18
N V	1242.8040	1242.9818	42.90	6.39	59	21
Si IV	1393.7550	1393.9778	47.92	6.09	39	19
C IV.....	1548.2020	1548.4797	53.78	4.08	210	35
C IV.....	1550.7740	1551.0459	52.55	7.65	236	33
O V	1371.2920	1371.5463	55.59	3.56	97	18
		$\langle V \rangle$	+50.10	1.10		
WD 1634−573:						
Si IV	1393.7550	1393.7531	−0.42	5.97	22	10
Si IV	1402.7770	1402.7963	4.12	5.89	17	9
C IV.....	1548.2020	1548.2069	0.95	3.61	90	14
C IV.....	1550.7740	1550.7710	−0.59	3.49	88	14
		$\langle V \rangle$	+0.61	2.15		
WD 1645+325:						
C II	1335.7076	1335.7767	15.51	5.41	83	26
He II.....	1640.5050	1640.5728	12.38	5.16	113	48
		$\langle V \rangle$	+13.87	3.73		
WD 1821+643:						
N V	1238.8210	1238.6111	−50.81	4.51	115	28
N V	1242.8040	1242.5930	−50.88	4.44	154	35
Si IV	1393.7550	1393.5588	−42.19	4.73	124	34
C IV.....	1548.2020	1547.9132	−55.93	5.92	110	67
C IV.....	1550.7740	1550.5522	−42.88	4.67	228	47
		$\langle V \rangle$	−48.07	2.14		
WD 2117+342:						
C IV.....	1230.5210	1230.6720	36.79	10.49	22	15
C IV.....	1261.7660	1262.0378	64.59	9.67	14	9
C IV.....	1315.6250	1315.8541	52.21	4.53	39	12
C IV.....	1342.5200	1342.7286	46.59	6.02	22	11
C IV.....	1344.1780	1344.4147	52.79	11.81	104	20
C IV.....	1351.2159	1351.3859	37.70	7.56	102	18
C IV.....	1352.9750	1353.2156	53.31	10.15	141	23
C IV.....	1440.2830	1440.4298	30.57	8.17	41	19
		$\langle V \rangle$	+47.22	2.62		

circumstellar lines will be discussed in more detail in a subsequent paper.

Evidence for mass loss is much more widespread in He-rich degenerate stars, in particular the hot DO and PG1159 spectral types. Fritz, Leckenby, & Sion (1990a) searched for evidence of ongoing mass loss in three DO degenerates, PG 1159−035, PG 1034+001, and KPD 0005+5106. They found some tentative indications of non-

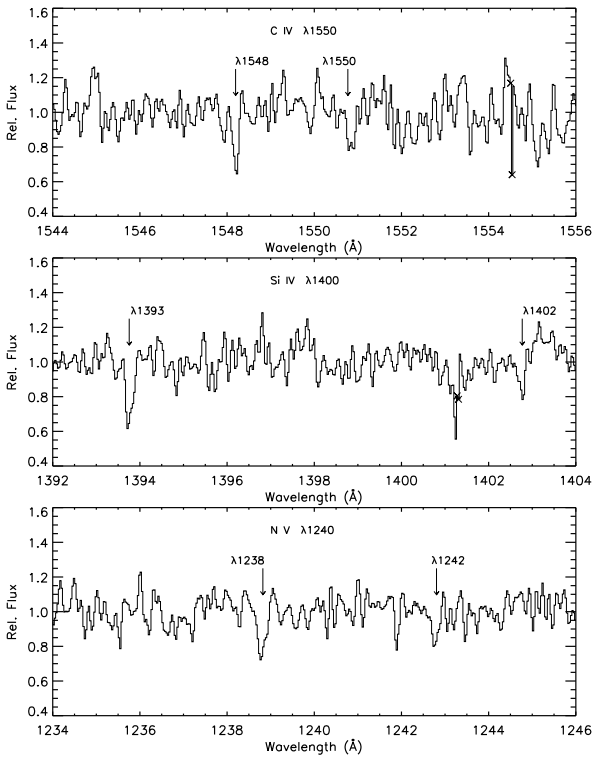

FIG. 6.—Co-added spectrum of the DA star GD 659 showing wavelength ranges containing the N v, C iv, and Si iv resonance lines. These lines, which are redshifted with respect to the stellar photosphere, are believed to arise in a circumstellar zone some distance from the star. The NEWSIPS spectrum can be compared with Fig. 3 of Holberg et al. (1995b).

photospheric features but no convincing evidence of ongoing mass loss. There now exist good examples of the presence of blueshifted features in the strong resonance lines of nearly all the hot DO stars observed with *IUE*. In some cases, such as NGC 246, and KPD 0005+5106, the blueshifted features actually dominate the photospheric N v, Si iv, or C iv resonance lines; in other stars, such as PG 1034+001 and PG 1159−035, they form separate detached features. In Figure 8 we show an example of photospheric and blueshifted C iv resonance line features in PG 1159−035. The origin of these blueshifted components is believed to be ongoing mass loss in the form of radiatively driven stellar winds. Such winds selectively remove heavy ions from the photosphere and must play an important role in determining the chemical evolution of the photosphere. In at least one star, REJ 0503−289, we also clearly see evidence of variability in both the strength and position of the C iv and Si iv lines among our four spectra. Spectral variability and mass loss events have previously been reported in the much hotter planetary nebula central stars K1-16 (Feibelman et al. 1995) and Longmore 4 (Werner et al. 1992).

4.1.2. *Interstellar Features*

Narrow interstellar features can be found in virtually all SWP echelle spectra of hot white dwarfs. Most commonly these are due to a well known set of lines consisting of the N i triplet at 1200 Å, O i λ1302, C ii λλ1334, 1335, Si ii λλ1190, 1193, 1260, 1304, 1526, and S ii λλ1250, 1253, 1259. Occasionally other features due to Si iii, Al ii, Mg ii, and Fe ii can be identified, and in a few stars, such as KPD 0005+5601 (Sion et al. 1997), where the line of sight passes through a diffuse cloud whose interior is shielded from the ionizing interstellar UV radiation field, features due to C i and Cl i can exist (see Fig. 9).

IUE has insufficient spectral resolution to resolve most interstellar lines; consequently, nearly all white dwarfs exhibit only a single ISM velocity component. It is very likely that most ISM features seen with *IUE* contain unresolved velocity structure corresponding to different "clouds" within the local ISM. However, in spite of this caveat, the lines of sight to the majority of white dwarfs observed with *IUE*, in echelle mode, lie at distances of

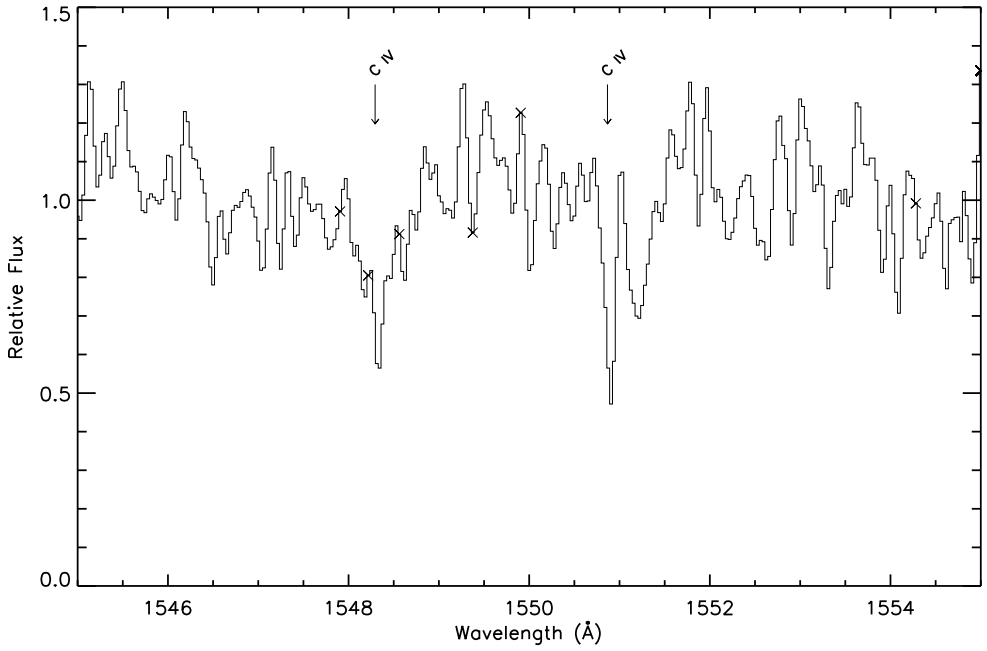

FIG. 7.—Co-added spectrum of the hot DA REJ 0457−281 showing the wavelength range containing the C iv resonance lines. The arrows indicate blueshifted circumstellar C iv features at +17.4 km s^{-1}. The photosphere is defined by N v, Si iv, and C iv resonance lines at +70.2 km s^{-1} (see Table 4).

TABLE 5

CIRCUMSTELLAR LINES

WD Number/ Species	Lab. (λ) Å	Obs. (λ) Å	V (km s^{-1})	σ (km s^{-1})	EW (mÅ)	σ (mÅ)
H-rich Degenerates						
WD 0050−332:						
N v	1238.8210	1238.9750	37.25	4.30	66	13
N v	1242.8040	1242.9563	36.75	5.80	35	13
Si iv	1393.7550	1393.9584	43.74	3.15	75	13
Si iv	1402.7770	1402.9368	34.15	5.27	38	12
C iv.....	1548.2020	1548.4008	38.48	4.10	60	17
C iv.....	1550.7740	1551.0520	53.73	7.24	51	20
		$\langle V \rangle$	+40.31	1.83		
WD 0232+035:						
C iv.....	1548.2020	1548.2029	0.17	2.84	73	9
C iv.....	1550.7740	1550.7699	−0.80	2.41	54	8
		$\langle V \rangle$	−0.40	1.84		
WD 0455−282:						
Si iv	1393.7550	1393.8066	11.11	5.22	35	13
Si iv	1402.7770	1402.8844	22.96	6.86	24	14
C iv.....	1548.2020	1548.3163	22.12	5.57	77	23
C iv.....	1550.7740	1550.8430	13.33	4.43	69	20
		$\langle V \rangle$	+16.21	2.66		
WD 1337+705:						
C ii	1334.5323	1334.4675	−14.56	4.56	74	19
C ii	1335.7076	1335.6670	−9.12	2.69	144	17
		$\langle V \rangle$	−10.52	2.31		
WD 1620−391:						
Si ii*.....	1264.7377	1264.9307	45.75	1.83	46	5
Si ii*.....	1265.0020	1265.1776	41.63	3.10	29	5
Si ii*.....	1309.2758	1309.4645	43.21	3.58	16	4
Si ii*.....	1533.4312	1533.6729	47.25	3.73	22	6
Si ii	1190.4158	1190.6282	53.49	9.87	30	15
Si ii	1260.4221	1260.5897	39.86	2.06	35	4
Si ii	1304.3702	1304.5637	44.47	4.31	17	5
Si ii	1526.7065	1526.9446	46.74	3.14	14	5
Si iii	1206.5220	1206.6909	41.98	9.49	72	36
Si iii	1294.5430	1294.7361	44.72	2.59	17	3
Si iii	1296.7260	1296.9219	45.30	3.20	14	4
Si iii	1298.9510	1299.1248	40.09	1.64	37	4
Si iii	1301.1460	1301.3392	44.52	5.01	12	4
Si iv	1393.7550	1393.9637	44.90	3.04	22	5
Si iv	1402.7770	1402.9734	41.98	4.05	16	5
C ii	1334.5323	1334.7262	43.55	2.77	22	4
C ii	1335.7076	1335.8856	39.95	1.51	31	3
Al iii	1854.7159	1854.9874	43.88	1.76	20	3
Al iii	1862.7900	1863.1215	53.34	3.07	16	4
		$\langle V \rangle$	+43.19	0.60		
He-rich Degenerates						
WD 0005+511:						
N v	1238.8210	1238.7832	−9.16	2.21	64	7
N v	1242.8040	1242.7869	−4.12	2.94	75	9
Si iv	1393.7550	1393.7244	−6.59	2.39	95	11
Si iv	1402.7770	1402.7233	−11.48	3.90	56	12
C iv.....	1548.2020	1548.1862	−3.07	2.57	177	17
C iv.....	1550.7740	1550.7477	−5.10	1.85	177	16
		$\langle V \rangle$	−6.19	1.00		
WD 0044−121:						
N v	1238.8210	1238.5480	−66.08	2.40	157	4
N v	1242.8040	1242.5249	−67.31	2.80	170	5
Si iv	1393.7550	1393.4252	−70.95	1.75	119	4
Si iv	1402.7770	1402.4397	−72.08	2.50	88	5
C iv.....	1548.2020	1547.8044	−76.99	4.12	483	10
C iv.....	1550.7740	1550.3993	−72.45	4.28	431	8
		$\langle V \rangle$	−70.18	1.05		
WD 0501−289:						
C iv.....	1550.7740	1550.6694	−20.22	5.75	81	16
O v	1371.2920	1371.2828	−2.00	6.51	30	14
		$\langle V \rangle$	−12.24	4.31		
WD 1034+001:						
He ii	1640.5050	1640.5406	6.51	6.31	82	20
Si iv	1393.7550	1394.7948	8.56	4.94	79	16
Si iv	1402.7770	1402.7974	4.36	6.49	26	9

TABLE 5—*Continued*

WD Number/ Species	Lab. (λ) Å	Obs. (λ) Å	V (km s^{-1})	σ (km s^{-1})	EW (mÅ)	σ (mÅ)
C IV.....	1548.2020	1548.2383	7.02	6.52	113	23
C IV.....	1550.7740	1550.8047	5.92	4.46	52	10
		$\langle V \rangle$	+6.60	2.47		
WD 1159−034:						
N V	1238.8210	1238.7977	−5.64	4.55	41	18
C IV.....	1548.2020	1548.2340	6.19	6.63	301	52
C IV.....	1550.7740	1550.7653	−1.70	7.65	283	55
		$\langle V \rangle$	−1.82	3.37		
WD 2117+342:						
C II*	1335.7076	1335.6393	−15.34	1.86	106	8
N V	1238.8210	1238.7538	−16.28	1.91	154	10
N V	1242.8040	1242.7513	−12.69	2.86	138	13
Si IV	1393.7550	1393.7069	−10.35	2.68	97	12
Si IV	1402.7770	1402.7255	−11.01	4.36	70	15
C IV.....	1548.2020	1548.1504	−10.00	2.15	314	21
C IV.....	1550.7740	1550.7346	−7.62	2.88	280	17
		$\langle V \rangle$	−11.90	1.08		

between 25 and 75 pc and are thus likely to be among the stars having the least complicated lines of sight observed with *IUE*. Although a wealth of data pertaining to the ISM is contained in the *IUE* white dwarf archives, surprisingly little work of a comprehensive nature has been published. Bruhweiler & Kondo (1982, 1983) and Bruhweiler & Vidal-Madjar (1987) discuss ISM velocities and H I column densities derived from ISM lines, such as N I and Si II, in five nearby white dwarfs. Jelinsky (1988) applied curve-of-growth techniques to the ISM lines in eight white dwarfs; however, some of the lines he considered are now known to be of stellar origin. The results presented in Tables 6 and 7 are, to our knowledge, the only large-scale compilation of ISM lines found in the white dwarfs observed with *IUE*.

The ISM features seen with *IUE* range in strength from a few 10s to a few 100s of mÅ in equivalent width and from -39 to $+23$ km s^{-1} in velocity. In Table 6 we present the relevant interstellar parameters for the sight lines to each star. The second column gives the distance to each object as a decimal fraction, if the estimate derives from an astrometric parallax (Hipparcos Catalog 1997 or van Altena, Lee, & Hoffliet 1991) or rounded to the nearest parsec, if based on a photometric parallax. The third and fourth columns give the Galactic coordinates for each star. The fifth column gives the mean velocity of the primary ISM velocity component observed with *IUE*. The sixth column gives an estimate of the log of the interstellar H I column density, if it is known. This quantity should correlate strongly with the strengths of interstellar features observed with *IUE*. For example, in those stars with log (N_H) < 18, observed ISM lines are very weak, often with only two or three of the strongest such as Si II λ1260, O I λ1302, and C II λ1334 detected. Unfortunately, the latter two features frequently suffer from their proximity to SWP reseau marks.

In Table 7 we list the ISM features that were identified in the spectra as distinct lines. Only those lines belonging to the standard set of lines discussed above are listed in Table 7. If additional lines are present or if there is a second

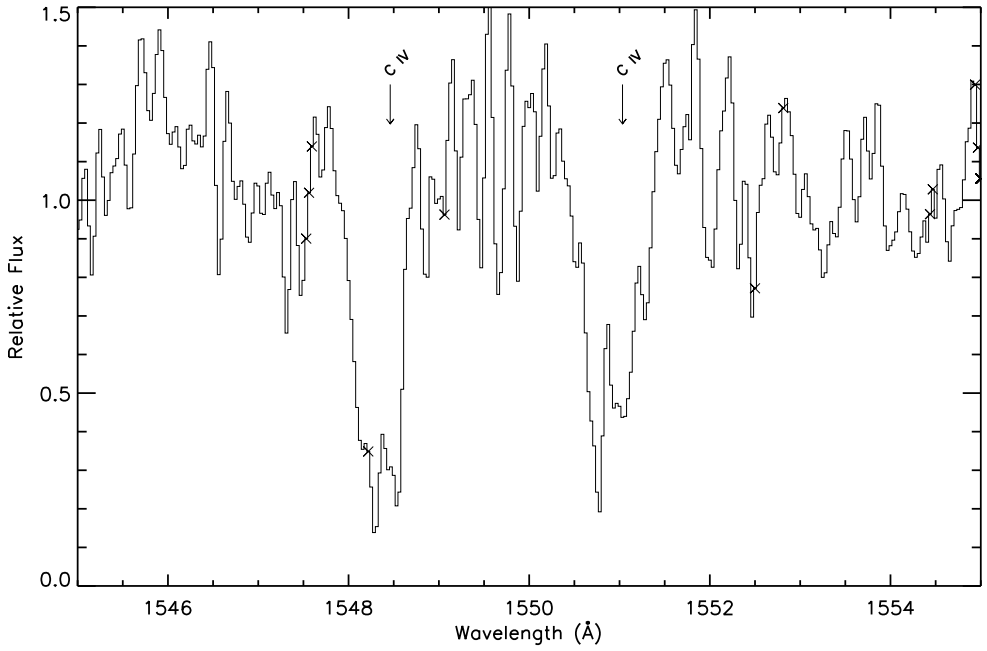

FIG. 8.—Co-added spectrum of the hot DOZ star PG 1159−035 showing the region of the C IV resonance lines. The self-reversed structure of these lines is due to the presence of the stellar photosphere at +50.1 km s^{-1} (*arrows*) and blueshifted wind features at −0.4 km s^{-1}.

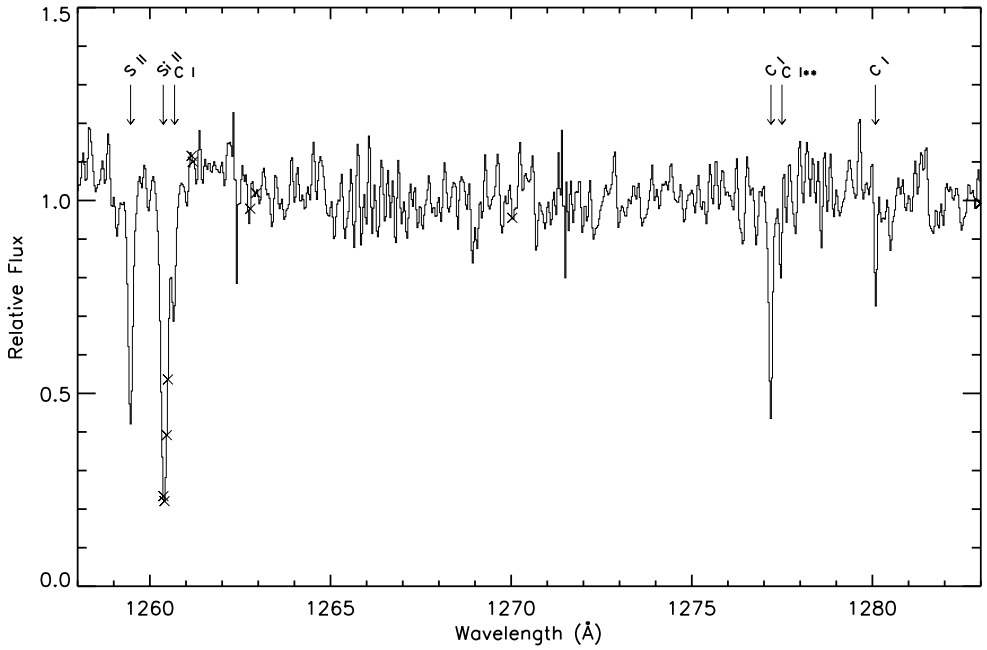

FIG. 9.—Co-added spectrum of the hot DOZ degenerate star KPD 0005+5106 showing the 1258–1283 Å region, which reveals two components of the ISM. The C I lines arise in a neutral cloud having a distinct velocity from that of the S II and Si III lines which are characteristic of the general ISM.

identifiable velocity component we note this in the discussions of individual stars. The laboratory wavelengths in Table 7 are taken from Morton (1991). The observed wavelengths correspond to the centroids of measurable features. The heliocentric velocity derived from these wavelengths and the corresponding uncertainty in velocity are given along with the observed equivalent widths and uncertainties. Finally, a weighted mean velocity for the component is computed from the lines available for each star. It should be realized that uncertainty in the mean velocity is an internal statistic and that the true velocity uncertainty is dominated by external factors such as the location of the star within the SWP large aperture and zero point of the SWP velocity scale. Comparisons with velocities independently known from other sources indicate that the *IUE* velocity measurements are generally accurate to within 3–5 km s^{-1}. Further investigations of the complete interstellar line data set will be presented elsewhere.

4.1.3. *Individual Stars*

GD 659.—High-ionization species (N V, Si IV, and C IV) are clearly seen in the *IUE* spectrum at +40 km s^{-1} (see Fig 6). Holberg et al. (1995a) argue, however, that these lines are due to highly excited circumstellar or interstellar gas. The stellar photosphere itself is apparently devoid of heavy elements.

Feige 24.—This is a pre-CV system consisting of a low-mass DA and a dMe main-sequence companion with an orbital period of 4.2316 days. The white dwarf contains a number of heavy elements including Fe and Ni (Vennes et al. 1992; Werner & Driezler 1994). In addition to photospheric features and ISM lines, Vennes et al. (1991) and Vennes & Thorstensen (1994) note the presence of transient He II absorption near inferior conjunction and C IV doublet features that arise from circumstellar gas or a red dwarf wind. Because an accurate ephemeris exists (Vennes & Thorstensen), co-additions have been performed in both the stellar and interstellar rest frames. For the stellar co-addition, nine spectra were selected so that the Doppler velocity of the stellar C IV lines did not impinge in the circumstellar C IV lines.

V471 Tau.—This is a pre-CV system consisting of a 34,000 K DA and K2 V primary. Sion et al. (1989) analyzed a series of SWP and LWP echelle spectra, and Mullan et al. (1989), using LWP spectra, found evidence of an expanding shell of gas at 1200 km s^{-1} around V471 Tau. Bruhweiler & Sion (1986) and Sion et al. (1989) report lower velocity (−590 km s^{-1}) components in O I, Si II, and C II, possibly a wind from the K2 dwarf. Mullan et al. (1991) report no detection of C or Si in the white dwarf photosphere, in spite of the fact that the white dwarf must accrete such species from the wind. It is now known (Sion et al. 1998) that such accretion occurs onto the magnetic poles of the white dwarf and that the earlier nondetection is explained by low fractional coverage of the poles and duty cycle of the pole visibility. Sion et al. (1998) observed Si II λ1206 in *HST* GHRS spectra of V471 Tau to be modulated at the 9.25 minute rotational period of the white dwarf. The implied accretion rate is 5 orders of magnitude below the Bondi-Hoyle fluid rate, which argues strongly for a magnetic-centrifugal propeller mechanism that severely limits accretion onto the white dwarf. Several types of SWP echelle spectra were obtained, including three velocity-compensated exposures in which the star was moved within the SWP aperture to compensate for orbital velocity and one long exposure (one-half an orbital period). Finding reliable ISM lines to register the spectra is quite difficult. We used only five uncompensated spectra for co-addition in the ISM frame.

40 Eri B.—This is a well-studied 16,400 K DA. No stellar features are seen; only weak interstellar features due to Si II λ1260, C II λ1334, and O I λ1302 are present. Like V471 Tau, few reliable ISM lines are available for co-addition.

S216.—Also designated LS V +46 21, S216, is a DAO1 star possessing an old planetary nebula. The existence of the Fe VII lines in this star were first reported by Feibelman &

TABLE 6

INTERSTELLAR PARAMETERS

WD Number	Distance (pc)	l (deg)	b (deg)	V (km s^{-1})	σ (km^{-1})	log N_H (cm^{-2})	σ (cm^{-2})
H-rich Degenerates							
WD 0004+330.....	97	112.48	−28.69	+0.10	1.53	<19.8	...
WD 0050−332.....	58	299.13	−84.10	+12.17	1.45	18.4	0.1
WD 0205+250.....	30	144.22	−34.42	+3.91	4.01	...	...
WD 0232+035.....	74.4	165.96	−50.27	−3.22	0.97	18.48	0.02
WD 0346−011.....	29	188.95	−40.10	+5.23	3.47	17.94	0.02
WD 0347+171.....	46.8	172.48	−27.94	+15.93	1.92	18.2	...
WD 0413−077.....	5.0	200.74	−37.98	+7.23	0.83	17.85	0.10
WD 0441+467.....	110	158.49	+0.47	−2.24	0.66	...	...
WD 0455−282.....	102	222.29	−36.77	+13.64	1.82	18.06	0.02
WD 0501+527.....	68.8	155.95	+7.10	+13.02	0.89	18.3	...
WD 0512+326.....	87	173.30	−3.36	+15.41	2.93	18.95	0.05
WD 0549+158.....	49	192.03	−5.39	+23.19	2.50	17.92	...
WD 0621−376.....	78	245.41	−21.43	+19.48	0.85	18.05	0.15
WD 0642−166.....	2.6	227.22	−8.88	+7.87	1.12	17.72	0.1
WD 0644+375.....	15.4	178.28	+15.43	+12.35	1.98	...	...
WD 1013−050.....	127	247.98	+40.45	−0.29	1.82	19.4	...
WD 1031−114.....	31	257.68	+38.79	−1.38	2.40	19	...
WD 1134+300.....	15.3	199.27	+73.46	−3.99	5.17	...	...
WD 1148−230.....	70	285.29	+37.44	−2.67	0.85	...	...
WD 1202+608.....	200	133.11	+55.66	−16.09[a]	2.32	...	...
WD 1210+533.....	87	135.61	+63.12	−7.79	1.69	...	...
WD 1234+481.....	129	129.81	+69.01	−28.85	1.92	19.13	0.13
WD 1254+223.....	73	317.27	+84.75	−11.07	2.96	17.92	0.1
WD 1314+293.....	68	54.11	+84.16	−17.42	2.48	17.94	0.02
WD 1337+705.....	24.8	117.17	+46.31	−1.73	3.40	...	...
WD 1615−154.....	55	358.80	+24.18	−38.19	1.79	...	...
WD 1620−391.....	12.9	341.53	+7.25	−24.98	1.17	<19.32	...
WD 1631+781.....	67	111.30	+33.58	−11.78	1.18	19.3	...
WD 1800+685.....	159	98.73	+29.78	−15.86	2.00	18.86	...
WD 1845+019.....	44	34.25	+1.74	−28.01	2.08	18.45	...
WD 2004−605.....	52	336.6	−32.9	−10.00	2.21	19.32	...
WD 2028+390.....	17.8	78.16	+0.06	−13.04	2.77	18.4	...
WD 2032+248.....	14.8	67.23	−9.02	−14.85	1.50	...	...
WD 2111+498.....	50	91.37	+1.14	−6.18	1.46	18.6	...
WD 2211−495.....	53	345.79	−52.62	−0.71	0.88	18.3	...
WD 2309+105.....	79	87.25	−45.11	−7.87	0.73	19.12	...
WD 2331−475.....	82	334.84	−64.81	+14.93	1.18	<17.9	...
WD 2350−706.....	116	309.91	−45.94	−2.87	3.12	...	...
He-rich Degenerates							
WD 0005+511.....	270	116.10	−10.91	−7.50[b]	0.76	20.7	0.1
WD 0044−121.....	900	118.87	−74.71	−4.27	0.89	20.3	...
WD 0501−289.....	90	230.67	−34.94	+18.13	1.93	17.88	0.13
WD 1034+001.....	100	247.55	+47.75	−0.77	0.98	...	...
WD 1159−034.....	440	279.82	+56.87	−17.73	1.06	20.0	0.1
WD 1211+332.....	115	175.04	+80.03	−17.97	1.88	...	...
WD 1634−573.....	37.1	329.88	−7.02	−22.72	0.99	18.8	0.02
WD 1645+325.....	36.0	54.08	+39.19	−27.12	4.66	...	...
WD 1821+643.....	1600	94.03	+27.43	−18.45[c]	1.12	...	...
WD 2117+342.....	1400	80.36	−10.41	−2.39	0.72	20.5	...

[a] A second set of higher velocity ISM lines present at −56 km s^{-1}.
[b] Contains a distinct set of low ionization C I lines (Sion et al. 1997)
[c] A second set of higher velocity ISM lines present at −48 km s^{-1}.

Bruhweiler (1990). Tweedy & Napiwotzki (1992) present a detailed analysis of the echelle spectrum SWP 27558 in which they list a number of photospheric features corresponding to a wide range of heavy ions, including Fe VI and Fe VII. Our co-added spectrum confirms many of these identifications. With respect to its high heavy element content, S216 resembles very much the somewhat cooler DAO star Feige 55.

REJ 0457−281.—This is a metal-rich, $T_{\rm eff} = 57{,}200$ K DA white dwarf. Its *IUE* spectrum shows N V, C IV, and Si IV resonance lines and its ORFEUS (900–1200 Å) spectrum shows excited Si IV lines and a single P V line (Vennes et al. 1996). Our NEWSIPS spectrum clearly reveals that the photospheric Si IV and C IV resonance lines are accompanied by features that are blueshifted by 53 km s^{-1} with respect to the stellar photosphere, indicating that, like REJ 1614−085, this DA is undergoing mass loss (see Fig. 7).

G191-B2B.—This is the prototypical hot metal-rich DA star in which numerous discoveries of various heavy elements were first made. Bruhweiler & Kondo (1981) first observed the N V, C IV, and Si IV resonance lines in G191-B2B. This was followed by Tweedy (1991) and Vennes et al. (1992) with *IUE* and Sion et al. (1992) with *HST* who all found features due to Fe V, and in the latter *HST* paper,

TABLE 7

INTERSTELLAR LINES

WD Number/ Species	Lab. (λ) Å	Obs. (λ) Å	V (km s^{-1})	σ (km s^{-1})	EW (mÅ)	σ (mÅ)
		H-rich Degenerates				
WD 0004+330:						
N I.....	1199.5496	1199.5173	−8.05	8.69	95	42
N I.....	1200.7098	1200.7172	1.83	5.64	105	38
Si II.....	1190.4158	1190.4343	4.67	7.60	53	35
Si II.....	1193.2897	1193.3114	5.46	5.38	103	33
Si II.....	1260.4221	1260.4071	−3.57	2.88	97	14
Si II.....	1304.3702	1304.3615	−2.02	7.07	77	26
Si II.....	1526.7065	1526.7365	5.87	4.16	94	28
Si III	1206.5000	1206.5194	4.82	8.07	67	30
S II.....	1259.5190	1259.5232	0.99	3.72	49	13
S II.....	1253.8110	1253.8091	−0.47	6.50	47	20
S II.....	1250.5840	1250.5508	−7.96	6.59	67	19
		$\langle V \rangle$	+0.10	1.53		
WD 0050−332:						
N I.....	1199.5496	1199.5854	8.97	6.30	72	24
C II	1334.5323	1334.5800	10.69	3.20	92	14
Si II.....	1190.4158	1190.4570	10.39	6.99	67	27
Si II.....	1193.2897	1193.3611	17.94	9.52	57	29
Si II.....	1260.4221	1260.4739	12.31	2.14	90	9
Si II.....	1304.3702	1304.4272	13.10	7.47	32	14
Si II.....	1526.7065	1526.7777	13.98	3.49	49	15
		$\langle V \rangle$	+12.17	1.45		
WD 0205+250:						
C II	1334.5323	1334.5352	0.63	5.52	106	38
C II	1335.7076	1335.7394	7.12	8.27	45	29
Si II.....	1260.4221	1260.4557	7.98	8.20	70	36
		$\langle V \rangle$	+3.91	4.01		
WD 0232+035:						
N I.....	1199.5496	1199.5636	3.51	4.97	61	8
N I.....	1200.2233	1200.2161	−1.80	4.84	41	9
N I.....	1200.7098	1200.7266	4.18	7.80	42	8
C II	1334.5323	1334.5133	−4.28	2.78	120	25
Si II.....	1190.4158	1190.4149	−0.22	3.60	40	9
Si II.....	1193.2897	1193.2965	1.72	4.25	48	9
Si II.....	1260.4221	1260.4008	−5.08	1.65	70	4
Si II.....	1304.3702	1304.3457	−5.64	3.40	32	6
Si II.....	1526.7065	1526.7159	1.85	3.01	49	8
Si III	1206.5000	1206.4852	−3.67	4.26	24	6
S II.....	1259.5190	1259.4833	−8.51	3.40	29	5
		$\langle V \rangle$	−3.22	0.97		
WD 0346−011:						
C II	1334.5323	1334.5294	−0.66	4.51	65	21
Si II.....	1260.4221	1260.4650	10.19	13.44	32	24
Si II.....	1526.7065	1526.7799	14.41	5.92	64	34
		$\langle V \rangle$	+5.23	3.47		
WD 0347+171:						
C II	1334.5323	1334.6046	16.23	2.07	68	11
Si II.....	1260.4221	1260.4812	14.05	5.14	47	13
		$\langle V \rangle$	+15.93	1.92		
WD 0413−077:						
O I.....	1302.1685	1302.1825	3.23	3.52	39	8
C II	1334.5323	1334.5638	7.07	0.92	90	4
Si II.....	1260.4221	1260.4561	8.07	2.73	33	6
Si II.....	1526.7065	1526.7775	13.93	4.13	16	5
		$\langle V \rangle$	+7.23	0.83		
WD 0441+467:						
N I.....	1199.5496	1199.5530	0.85	2.13	108	12
N I.....	1200.2233	1200.2262	0.73	2.82	106	13
N I.....	1200.7098	1200.7090	−0.21	3.27	93	14
O I.....	1302.1685	1302.1437	−5.70	3.20	128	9
C II	1334.5323	1334.5295	−0.63	2.02	164	7
C II	1335.7076	1335.6764	−7.01	2.30	105	5
Si II.....	1190.4158	1190.4072	−2.15	4.14	92	17
Si II.....	1193.2897	1193.2998	2.55	3.77	77	13
Si II.....	1260.4221	1260.3966	−6.07	2.44	146	6
Si II.....	1304.3702	1304.3566	−3.14	2.15	70	8
Si II.....	1526.7065	1526.7081	0.31	2.20	119	12
S II.....	1259.5190	1259.4941	−5.93	1.87	57	6
S II.....	1250.5840	1250.5844	0.09	2.01	57	6
Al II.....	1670.7874	1670.7788	−1.53	3.86	101	17
		$\langle V \rangle$	−2.24	0.66		

TABLE 7—*Continued*

WD Number/ Species	Lab. (λ) Å	Obs. (λ) Å	V (km s^{-1})	σ (km s^{-1})	EW (mÅ)	σ (mÅ)
WD 0455−282:						
Si II	1260.4221	1260.4723	11.93	2.88	104	11
Si II	1304.3702	1304.4597	20.57	6.23	33	14
Si II	1526.7065	1526.7839	15.20	3.87	77	17
Si III	1206.5000	1206.5514	12.77	3.35	112	17
		$\langle V \rangle$	+13.64	1.82		
WD 0501+527:						
N I	1199.5496	1199.5941	11.14	3.04	40	7
N I	1200.2233	1200.3031	19.94	2.95	41	7
N I	1200.7098	1200.7726	15.67	4.32	36	8
O I	1302.1685	1302.2083	9.16	3.35	69	4
Si II	1190.4158	1190.4773	15.49	4.31	39	9
Si II	1193.2897	1193.3408	12.85	2.66	47	6
Si II	1260.4221	1260.4562	8.10	2.20	69	4
Si II	1304.3702	1304.4113	9.43	3.27	34	6
Si II	1526.7065	1526.7845	15.32	2.21	63	7
Si III	1206.5000	1206.5497	12.35	3.36	23	6
Al II	1670.7874	1670.8824	17.06	3.01	37	8
		$\langle V \rangle$	+13.02	0.89		
WD 0512+326:						
N I	1200.2233	1200.2965	18.29	6.49	77	35
N I	1200.7098	1200.7988	22.22	11.46	67	43
O I	1302.1685	1302.2095	9.44	7.66	98	21
Si II	1260.4221	1260.4799	13.73	4.88	90	17
Si II	1304.3702	1304.4492	18.15	7.60	43	20
Si II	1526.7065	1526.7874	15.87	10.63	76	43
		$\langle V \rangle$	+15.41	2.93		
WD 0549+158:						
O I	1302.1685	1302.2794	25.55	3.09	40	11
Si II	1190.4158	1190.5312	29.08	7.69	53	26
Si II	1260.4221	1260.4810	13.99	5.15	40	10
		$\langle V \rangle$	+23.19	2.50		
WD 0621−376:						
N I	1199.5496	1199.6151	16.38	2.64	85	9
N I	1200.2233	1200.3152	22.96	2.41	54	8
N I	1200.7098	1200.7988	22.22	2.18	64	8
C II	1334.5323	1334.5950	14.07	3.24	104	4
C II	1335.7076	1335.7888	18.22	3.03	22	5
Si II	1190.4158	1190.5098	23.67	3.67	55	10
Si II	1193.2897	1193.3667	19.35	2.83	65	8
Si II	1260.4221	1260.4888	15.85	2.84	84	5
Si II	1304.3702	1304.4569	19.92	2.80	26	6
Si II	1526.7065	1526.8099	20.30	2.62	60	8
S II	1259.5190	1259.5800	14.50	7.19	9	5
Al II	1670.7874	1670.8955	19.41	5.56	26	11
		$\langle V \rangle$	+19.48	0.85		
WD 0642−166:						
O I	1302.1685	1302.1843	3.65	3.06	77	12
C II	1334.5323	1334.5676	7.93	1.32	121	4
Si II	1260.4221	1260.4707	11.56	2.97	50	9
		$\langle V \rangle$	+7.87	1.12		
WD 0644+375:						
O I	1302.1685	1302.2179	11.38	5.28	56	19
C II	1334.5323	1334.5923	13.46	2.80	68	12
Si II	1260.4221	1260.4691	11.18	3.30	44	13
		$\langle V \rangle$	+12.35	1.98		
WD 1013−050:						
N I	1199.5496	1199.5366	−3.23	10.67	124	53
N I	1200.2233	1200.2231	−0.03	7.76	159	50
C II	1334.5323	1334.5244	−1.78	2.47	93	18
Si II	1260.4221	1260.4164	−1.37	7.02	45	20
Si II	1304.3702	1304.4160	10.52	6.88	70	28
S II	1259.5190	1259.5341	3.57	4.60	54	17
S II	1253.8110	1253.7885	−5.40	6.47	60	21
		$\langle V \rangle$	−0.29	1.82		
WD 1031−114:						
O I	1302.1685	1302.1597	−2.02	3.57	74	19
C II	1335.7076	1335.7145	1.53	6.65	24	15
Si II	1260.4221	1260.4154	−1.60	3.70	80	17
		$\langle V \rangle$	−1.38	2.40		

TABLE 7—*Continued*

WD Number/ Species	Lab. (λ) Å	Obs. (λ) Å	V (km s^{-1})	σ (km s^{-1})	EW (mÅ)	σ (mÅ)
WD 1134+300:						
Si II	1260.4221	1260.4213	−0.20	8.65	43	23
Si II	1526.7065	1526.6755	−6.09	6.45	70	30
		$\langle V \rangle$	−3.99	5.17		
WD 1148−230:						
N I	1199.5496	1199.5496	0.00	6.80	148	52
N I	1200.2233	1200.1904	−8.20	6.67	148	49
N I	1200.7098	1200.7012	−2.16	7.56	113	48
C II	1335.7076	1335.6970	−2.38	1.78	75	9
Si II	1190.4158	1190.4202	1.11	8.56	95	46
Si II	1260.4221	1260.4048	−4.12	2.46	255	18
Si II	1304.3702	1304.3560	−3.28	4.52	155	24
Si II	1526.7065	1526.6968	−1.92	1.46	252	19
S II	1259.5190	1259.4910	−6.68	2.77	176	18
S II	1253.8110	1253.7985	−3.01	6.89	152	33
S II	1250.5840	1250.5844	0.09	3.46	70	17
Al II	1670.7874	1670.7810	−1.14	3.42	196	29
		$\langle V \rangle$	−2.67	0.85		
WD 1202+608:						
N I	1199.5496	1199.5157	−8.45	6.44	73	22
N I	1200.2233	1200.1897	−8.39	6.34	50	19
N I	1200.7098	1200.6432	−16.64	7.03	56	21
C II	1334.5323	1334.4281	−23.42	6.12	159	14
Si II	1190.4158	1190.3872	−7.19	13.17	50	45
Si II	1193.2897	1193.2258	−16.04	12.84	64	44
Si II	1260.4221	1260.3278	−22.44	5.41	172	13
Si II	1304.3702	1304.3182	−11.95	10.09	32	25
Si II	1526.7065	1526.6779	−5.63	10.40	74	36
Si III	1206.5000	1206.4075	−22.99	6.79	91	28
S II	1259.5190	1259.4640	−13.10	19.14	33	16
		$\langle V \rangle$	−16.09	2.32		
WD 1210+533:						
N I	1200.2233	1200.1967	−6.65	7.08	73	36
N I	1200.7098	1200.6735	−9.08	6.51	92	44
C II	1334.5323	1334.4998	−7.32	3.21	146	20
C II	1335.7076	1335.6536	−12.14	5.92	36	16
Si II	1190.4158	1190.3975	−4.61	5.67	87	39
Si II	1193.2897	1193.2292	−15.18	9.92	82	42
Si II	1260.4221	1260.3888	−7.93	2.79	113	16
Si II	1304.3702	1304.3630	−1.65	8.72	53	26
		$\langle V \rangle$	−7.79	1.69		
WD 1234+481:						
N I	1199.5496	1199.4620	−21.87	7.18	87	41
C II	1334.5323	1334.3643	−37.76	4.95	77	14
Si II	1260.4221	1260.2858	−31.44	2.92	95	16
Si II	1304.3702	1304.2905	−21.07	4.29	71	24
Si II	1526.7065	1526.5929	−22.32	5.87	121	28
Si III	1206.5000	1206.3539	−36.31	9.57	48	32
		$\langle V \rangle$	−28.85	1.92		
WD 1254+223:						
O I	1302.1685	1302.1392	−6.74	6.22	37	17
C II	1334.5323	1334.4890	−9.73	4.53	41	12
Si II	1260.4221	1260.3568	−15.53	5.03	24	9
		$\langle V \rangle$	−11.07	2.96		
WD 1314+293:						
C II	1334.5323	1334.4558	−17.19	3.52	46	8
Si II	1193.2897	1193.2230	−16.75	6.11	38	14
Si II	1260.4221	1260.3621	−14.28	6.33	25	8
S II	1259.5190	1259.4301	−21.18	5.75	19	7
		$\langle V \rangle$	−17.42	2.48		
WD 1337+705:						
Si II	1260.4221	1260.4150	−1.68	3.67	93	21
S II	1259.5190	1259.5106	−2.00	8.94	43	23
		$\langle V \rangle$	−1.73	3.40		
WD 1615−154:						
O I	1302.1685	1301.9957	−39.77	5.28	67	22
C II	1334.5323	1334.3723	−35.95	2.94	77	16
Si II	1260.4221	1260.2650	−37.37	5.31	101	19
Si II	1304.3702	1304.2260	−33.16	8.82	43	24
S II	1253.8110	1253.6455	−39.58	5.35	36	16

TABLE 7—*Continued*

WD Number/ Species	Lab. (λ) Å	Obs. (λ) Å	V (km s^{-1})	σ (km s^{-1})	EW (mÅ)	σ (mÅ)
S II	1250.5840	1250.4230	−38.60	7.25	30	16
Al II	1670.7874	1670.5515	−42.32	4.13	151	45
		$\langle V \rangle$	−38.19	1.79		
WD 1620−391:						
N I	1199.5496	1199.4542	−23.83	10.53	26	16
C II	1334.5323	1334.4055	−28.49	2.90	83	5
C II	1335.7076	1335.5991	−24.36	6.15	6	3
Si II	1190.4158	1190.3391	−19.31	8.84	29	14
Si II	1193.2897	1193.2025	−21.90	9.68	18	12
Si II	1260.4221	1260.2961	−29.61	2.86	48	4
Si II	1304.3702	1304.2664	−23.88	2.68	28	5
Si II	1526.7065	1526.6012	−20.69	2.53	35	6
S II	1259.5190	1259.4043	−27.31	4.03	22	4
S II	1253.8110	1253.6993	−26.71	8.44	12	6
Al II	1670.7874	1670.6654	−21.88	3.96	26	8
		$\langle V \rangle$	−24.98	1.17		
WD 1631+781:						
N I	1199.5496	1199.5162	−8.33	4.46	108	21
N I	1200.2233	1200.1875	−8.93	6.17	67	22
N I	1200.7098	1200.6787	−7.77	6.48	78	24
C II	1334.5323	1334.4718	−13.60	3.78	138	10
C II	1335.7076	1335.6307	−17.26	4.05	20	6
Si II	1190.4158	1190.4023	−3.38	6.26	56	21
Si II	1260.4221	1260.3591	−14.98	2.58	99	10
Si II	1304.3702	1304.3198	−11.59	5.04	44	12
Si II	1526.7065	1526.6848	−4.27	3.30	109	17
S II	1259.5190	1259.4539	−15.52	3.35	50	9
S II	1253.8110	1253.7504	−14.51	4.48	28	10
S II	1250.5840	1250.5499	−8.16	4.75	35	9
		$\langle V \rangle$	−11.78	1.18		
WD 1800+685:						
N I	1199.5496	1199.4935	−14.00	9.92	97	66
Si II	1260.4221	1260.3490	−17.39	3.90	194	29
Si II	1304.3702	1304.3334	−8.47	4.38	83	27
Si II	1526.7065	1526.6631	−8.53	7.03	64	39
Si III	1206.5000	1206.4199	−19.90	4.71	147	49
S II	1259.5190	1259.4266	−22.00	4.63	72	24
S II	1253.8110	1253.7517	−14.19	10.01	64	34
		$\langle V \rangle$	−15.86	2.00		
WD 1845+019:						
C II	1334.5323	1334.3701	−36.44	6.00	84	11
Si II	1260.4221	1260.2875	−32.03	3.26	63	13
Si II	1304.3702	1304.2797	−21.18	4.12	65	18
Si II	1526.7065	1526.6069	−21.19	5.69	77	25
S II	1259.5190	1259.4011	−28.07	7.09	32	14
		$\langle V \rangle$	−28.01	2.08		
WD 2004−605:						
N I	1199.5496	1199.5004	−12.30	7.95	73	38
Si II	1193.2897	1193.2677	−5.52	6.29	78	34
Si II	1260.4221	1260.3906	−7.49	4.09	68	15
Si II	1304.3702	1304.3300	−9.26	6.50	38	20
Si II	1526.7065	1526.6509	−10.93	5.12	66	26
S II	1259.5190	1259.4565	−14.88	4.82	40	14
		$\langle V \rangle$	−10.00	2.21		
WD 2028+390:						
C II	1334.5323	1334.4427	−20.13	6.08	97	18
C II	1335.7076	1335.6255	−18.44	5.03	27	13
Si II	1260.4221	1260.3937	−6.76	5.16	90	25
Si II	1526.7065	1526.6731	−6.57	6.18	139	40
		$\langle V \rangle$	−13.04	2.77		
WD 2032+248:						
C II	1334.5323	1334.4592	−16.43	3.20	115	7
Si II	1260.4221	1260.3528	−16.49	2.00	66	12
Si II	1304.3702	1304.3271	−9.90	5.09	50	14
Si II	1526.7065	1526.6643	−8.29	4.20	74	17
		$\langle V \rangle$	−14.85	1.50		
WD 2111+498:						
N I	1199.5496	1199.5220	−6.89	8.82	38	24
N I	1200.7098	1200.6998	−2.50	6.42	81	27
C II	1334.5323	1334.4905	−9.41	3.30	88	9

TABLE 7—*Continued*

WD Number/ Species	Lab. (λ) Å	Obs. (λ) Å	V (km s^{-1})	σ (km s^{-1})	EW (mÅ)	σ (mÅ)
Si II	1190.4158	1190.4001	−3.93	10.23	57	30
Si II	1193.2897	1193.2885	−0.31	7.21	102	30
Si II	1260.4221	1260.3977	−5.81	2.88	74	10
Si II	1304.3702	1304.3604	−2.27	6.00	36	14
Si II	1526.7065	1526.6788	−5.44	2.76	72	18
S II	1259.5190	1259.4688	−11.97	5.90	44	11
		$\langle V \rangle$	−6.18	1.46		
WD 2211−495:						
N I	1199.5496	1199.5432	−1.59	2.53	61	8
N I	1200.2233	1200.2272	0.98	3.34	47	8
N I	1200.7098	1200.7031	−1.68	3.70	45	9
C II	1334.5323	1334.5159	−3.70	2.74	133	4
Si II	1260.4221	1260.4225	0.09	1.86	119	4
Si II	1304.3702	1304.3579	−2.83	1.83	52	5
Si II	1526.7065	1526.7325	5.11	2.92	89	7
Al II	1670.7874	1670.7913	0.70	2.77	43	9
		$\langle V \rangle$	−0.71	0.88		
WD 2309+105:						
N I	1199.5496	1199.5243	−6.32	4.36	71	14
N I	1200.2233	1200.2344	2.77	4.30	72	14
N I	1200.7098	1200.6923	−4.39	5.52	70	16
O I	1302.1685	1302.1295	−8.97	1.82	92	8
C II	1335.7076	1335.6708	−8.27	3.19	21	5
Si II	1190.4158	1190.4056	−2.55	4.31	78	15
Si II	1193.2897	1193.2677	−5.52	3.02	72	13
Si II	1260.4221	1260.3843	−9.00	1.35	81	5
Si II	1304.3702	1304.3331	−8.53	2.01	47	7
Si II	1526.7065	1526.6747	−6.26	2.39	99	13
Si III	1206.5000	1206.4709	−7.22	6.43	22	10
S II	1259.5190	1259.4703	−11.59	3.15	29	6
S II	1253.8110	1253.7832	−6.66	8.16	13	8
S II	1250.5840	1250.5234	−14.51	5.05	12	6
Al II	1670.7874	1670.7688	−3.33	5.24	62	19
		$\langle V \rangle$	−7.87	0.73		
WD 2331−475:						
N I	1199.5496	1199.5878	9.55	3.55	107	19
N I	1200.2233	1200.2777	13.60	3.60	85	18
N I	1200.7098	1200.7800	17.54	5.32	51	19
C II	1335.7076	1335.7610	11.97	4.83	20	8
Si II	1190.4158	1190.4941	19.74	7.24	113	30
Si II	1193.2897	1193.3486	14.81	4.53	123	23
Si II	1260.4221	1260.4866	15.33	2.08	147	11
Si II	1304.3702	1304.4420	16.50	4.36	57	13
Si II	1526.7065	1526.7941	17.19	2.73	112	18
		$\langle V \rangle$	+14.93	1.18		
WD 2350−706:						
Si II	1260.4221	1260.4133	−2.09	3.39	102	17
S II	1253.8110	1253.7808	−7.24	8.00	35	20
		$\langle V \rangle$	−2.87	3.12		
He-rich Degenerates						
WD 0005+511:						
N I	1199.5496	1199.5363	−3.33	3.18	126	18
N I	1200.2233	1200.2075	−3.93	4.42	111	20
N I	1200.7098	1200.6738	−8.99	3.84	109	19
C II	1334.5323	1334.4889	−9.76	1.86	167	6
Si II	1190.4158	1190.4156	−0.03	5.97	83	24
Si II	1260.4221	1260.3982	−5.69	2.06	186	9
Si II	1304.3702	1304.3234	−10.77	2.01	105	10
Si II	1526.7065	1526.6810	−5.01	1.43	125	11
Si III	1206.5000	1206.4772	−5.67	6.30	94	20
S II	1259.5190	1259.4622	−13.54	4.12	98	9
S II	1253.8110	1253.7694	−9.95	3.27	76	10
S II	1250.5840	1250.5303	−12.88	3.96	73	7
		$\langle V \rangle$	−7.50	0.76		
WD 0044−121:						
N I	1200.2233	1200.2109	−3.08	3.74	110	7
N I	1200.7098	1200.7018	−2.01	3.93	114	8
C II	1334.5323	1334.4977	−7.79	2.30	178	4

TABLE 7—*Continued*

WD Number/ Species	Lab. (λ) Å	Obs. (λ) Å	V (km s^{-1})	σ (km s^{-1})	EW (mÅ)	σ (mÅ)
C II	1335.7076	1335.6711	−8.19	3.44	67	3
Si II	1260.4221	1260.4084	−3.25	2.66	194	3
Si II	1304.3702	1304.3459	−5.58	2.76	135	5
Si II	1526.7065	1526.7150	1.65	2.61	179	6
Si III	1206.5000	1206.4678	−8.01	5.01	95	5
S II	1259.5190	1259.5013	−4.21	2.96	106	4
S II	1253.8110	1253.7880	−5.52	3.23	94	4
S II	1250.5840	1250.5659	−4.33	3.62	66	4
Al II	1670.7874	1670.7745	−2.30	3.20	203	9
		$\langle V \rangle$	−4.27	0.89		
WD 0501−289:						
O I	1302.1685	1302.2852	26.87	7.16	82	14
Si II	1260.4221	1260.4950	17.33	2.07	92	9
Si II	1304.3702	1304.4541	19.27	8.20	20	13
		$\langle V \rangle$	+18.13	1.93		
WD 1034+001:						
N I	1199.5496	1199.5537	1.04	5.23	69	18
N I	1200.2233	1200.2207	−0.64	4.61	65	17
N I	1200.7098	1200.7004	−2.35	3.54	81	17
C II	1334.5323	1334.5134	−4.25	3.15	126	10
Si II	1190.4158	1190.4188	0.77	7.02	59	22
Si II	1193.2897	1193.2921	0.61	4.70	78	19
Si II	1260.4221	1260.4303	1.95	2.18	117	10
Si II	1304.3702	1304.3535	−3.84	3.62	64	12
Si II	1526.7065	1526.7139	1.44	3.96	88	19
Si III	1206.5000	1206.5045	1.12	3.01	83	13
S II	1259.5190	1259.4985	−4.88	4.34	62	11
S II	1253.8110	1253.8223	2.68	3.92	76	13
S II	1250.5840	1250.5591	−5.97	3.26	44	9
Al II	1670.7874	1670.7969	1.71	4.79	94	26
		$\langle V \rangle$	−0.77	0.98		
WD 1159−034:						
N I	1199.5496	1199.4735	−19.01	10.13	55	34
N I	1200.2233	1200.1389	−21.07	6.67	105	36
N I	1200.7098	1200.6709	−9.72	8.72	123	44
C II	1334.5323	1334.4470	−19.17	2.46	178	17
C II	1335.7076	1335.6200	−19.67	2.83	57	11
Si II	1190.4158	1190.3706	−11.38	5.78	90	36
Si II	1193.2897	1193.2283	−15.43	6.53	126	37
Si II	1260.4221	1260.3506	−17.01	2.82	179	16
Si II	1304.3702	1304.2646	−24.27	4.61	99	22
Si II	1526.7065	1526.6490	−11.29	4.26	139	30
Si III	1206.5000	1206.4442	−13.86	4.72	59	20
S II	1259.5190	1259.4324	−20.63	4.41	67	15
S II	1253.8110	1253.7368	−17.75	3.58	75	15
S II	1250.5840	1250.5103	−17.67	3.67	54	12
Al II	1670.7874	1670.7024	−15.24	6.75	97	41
		$\langle V \rangle$	−17.73	1.06		
WD 1211+332:						
N I	1199.5496	1199.4850	−16.14	7.38	77	39
N I	1200.2233	1200.1825	−10.18	8.34	72	42
N I	1200.7098	1200.6711	−9.66	7.20	78	44
C II	1334.5323	1334.4497	−18.57	2.83	146	25
Si II	1190.4158	1190.3376	−19.67	10.45	125	64
Si II	1193.2897	1193.2279	−15.52	15.10	120	79
Si II	1260.4221	1260.3474	−17.77	4.15	90	23
Si II	1304.3702	1304.2615	−25.00	8.25	61	33
S II	1259.5190	1259.4158	−24.58	7.00	85	29
		$\langle V \rangle$	−17.97	1.88		
WD 1634−573:						
N I	1199.5496	1199.4525	−24.25	3.66	51	13
N I	1200.2233	1200.1195	−25.92	6.54	49	16
N I	1200.7098	1200.6414	−17.10	7.84	45	17
C II	1334.5323	1334.4285	−23.34	1.85	89	7
Si II	1190.4158	1190.3551	−15.28	7.71	44	18
Si II	1260.4221	1260.3204	−24.19	1.73	78	6
Si II	1304.3702	1304.2715	−22.70	5.02	38	11
Si II	1526.7065	1526.6107	−18.82	2.52	48	11
S II	1259.5190	1259.4064	−26.82	5.38	28	8
Al II	1670.7874	1670.7034	−15.07	6.82	50	21
		$\langle V \rangle$	−22.72	0.99		

TABLE 7—*Continued*

WD Number/ Species	Lab. (λ) Å	Obs. (λ) Å	V (km s^{-1})	σ (km s^{-1})	EW (mÅ)	σ (mÅ)
WD 1645+325:						
Si II	1260.4221	1260.3109	−26.45	6.06	79	30
Si II	1260.4221	1260.3041	−28.08	7.29	83	33
		$\langle V \rangle$	−27.12	4.66		
WD 1821+643:						
N I	1200.7098	1200.6432	−16.64	6.49	223	67
C II	1334.5323	1334.4557	−17.22	1.50	168	21
C II	1335.7076	1335.5087	−14.74	5.69	63	44
Si II	1193.2897	1193.2209	−17.27	7.59	63	146
Si II	1260.4221	1260.3893	−7.81	5.30	113	68
Si II	1526.7065	1526.6473	−11.63	4.02	220	51
Si III	1206.5000	1206.4097	−22.45	4.88	325	52
S II	1259.5190	1259.4127	−25.31	6.93	103	30
S II	1253.8110	1253.6864	−29.80	4.74	103	30
S II	1250.5840	1250.4619	−29.26	5.78	56	25
Al II	1670.7874	1670.6400	−26.44	4.52	229	75
		$\langle V \rangle$	−18.45	1.12		
WD 2117+342:						
N I	1199.5496	1199.5599	2.59	5.21	136	23
N I	1200.2233	1200.2031	−5.03	4.26	106	20
N I	1200.7098	1200.6987	−2.77	4.39	92	20
C II	1334.5323	1334.5038	−6.42	4.32	208	47
Si II	1190.4158	1190.4381	5.63	5.49	96	26
Si II	1193.2897	1193.2922	0.64	3.35	143	21
Si II	1260.4221	1260.4214	−0.17	1.84	178	9
Si II	1304.3702	1304.3438	−6.09	3.55	118	14
Si II	1526.7065	1526.7220	3.04	2.01	150	15
Si III	1206.5000	1206.5000	0.00	3.46	66	14
S II	1259.5190	1259.4989	−4.79	1.57	104	8
S II	1253.8110	1253.7876	−5.60	2.29	92	10
S II	1250.5840	1250.5688	−3.63	2.33	65	8
Al II	1670.7874	1670.7539	−6.00	2.86	195	26
		$\langle V \rangle$	−2.39	0.72		

C III in *IUE* and *HST* FOS spectra of G191-B2B. Later Holberg et al. (1994) and Werner & Dreizler (1994) also identified features due to Ni V in G191-B2B and several other metal-rich DA white dwarfs. Vennes et al. (1996) also have found P V and S IV features in the 900–1200 Å ORFEUS spectrum of this star. Recently Lanz et al. (1996) used a co-added *IUE* echelle spectrum of this star to demonstrate a self-consistent NLTE model atmosphere that reproduced both the *IUE* heavy element abundances and the *EUVE* spectrum of G191-B2B. In a follow-up study of the joint effects of high metal abundance and NLTE atmospheres, Barstow et al. (1998) have shown that the traditional Balmer line temperatures of stars such as G191-B2B have been overestimated by from 4000 to 7000 K.

KW Aur C.—This $T_{\rm eff} = 47{,}000$ K DA was discovered as a *ROSAT* EUV source by Hodgkin et al. (1993) and is believed to reside in a binary system with a F4 V primary. The primary star is a single-line spectroscopic binary (orbital period = 2.99 days). Webbink et al. (1992) briefly discuss the *IUE* spectrum (SWP 45667) noting the lack of a He II λ1640 line. Our co-added spectrum, based on ISM lines, clearly shows the presence of the Si IV 1400 Å resonance lines, which we assume to be stellar and consistent with the EUV opacity noted by Vennes, Christian, & Thorstensen (1998). This makes it very unlikely that it is the white dwarf which is responsible for the observed binary motion.

REJ 0623−374.—This is one of the most extreme of the metal-rich DA white dwarfs. In spite of its relative brightness and high temperature, it exhibits a very sharply truncated short-wavelength EUV spectrum, which implies a high short-wavelength opacity. Holberg et al. (1993) analyzed its *IUE* echelle spectrum, determining that it had an even higher Fe abundance than G191-B2B. The authors linked the high levels of Fe abundance to the EUV opacity. REJ 0623−374 also was among the DA stars in which Werner & Driezler (1994) found traces of Ni. Our four-spectrum co-add of REJ 0623−374 represents a significant improvement over the previous single NEWSIPS spectra analyzed in Holberg et al. (1994).

GD 71.—Bruhweiler (1984) discussed the possible detection of the N V, C IV, and Si IV resonance lines in the DA star GD 71, which suggests that these are formed in a halo region near the star. VTS also noted the probable presence of the C IV resonance lines. We have examined our co-added GD 71 spectra as well as the individual spectra and can find no convincing evidence of any of the above resonance lines.

Sirius B.—A number of SWP echelle spectra were obtained of Sirius B during the early years of *IUE*, when the white dwarf was near its maximum separation from Sirius A. However, only four (one large aperture and three small aperture) spectra were determined to be usable in the study of Sirius B itself. Bruhweiler & Kondo (1982) detected interstellar O I λ1302, Si II λ1260, and C II λ1334 lines and used these to estimate the interstellar H I column to Sirius B. Holberg et al. (1998a) reexamined these data, refining the Bruhweiler & Kondo H I estimate. Our co-added spectrum clearly shows these features but apparently nothing else.

REJ 1016−053.—Like Feige 24, REJ 1016−053 is a pre-CV system (orbital period, 0.788929 days) containing a

hot H-rich white dwarf and a dMe companion, exhibiting variable emission lines resulting from a reflection effect. Unlike Feige 24, however, REJ 1016−053 contains photospheric He, which makes the white dwarf a DAO star. The physical properties of the system and the white dwarf are discussed in Thorstensen, Vennes, & Bowyer (1996). They show co-added echelle line profiles of the strong C IV resonance lines, which may have a circumstellar component, and the photospheric He II line. The three existing *IUE* spectra contain considerable Doppler smearing of the stellar component; therefore, only a co-addition in the ISM frame was done. In addition to the C IV and He II lines reported by Thorstensen et al., our co-added spectrum also shows Si IV and N V resonance lines. Because the profiles of these lines resemble that of the He II line we presume these to be predominantly photospheric. However, because only a detailed analysis could determine this, we have not listed these features in either Table 4 or 5.

EC 1148-2.—This is a bright hot DAO star discovered in the Edinburgh-Cape Blue Object Survey (O'Donoghue et al. 1993). The star has recently been reclassified as a DAOZ (Stys et al. 1999). A detailed discussion of the optical and far UV spectra of EC 1148-2 will be given in Stys et al. (1999).

Feige 55.—This star is one of the brightest of the DAO white dwarfs. Lamontagne et al. (1993) used the then existing *IUE* SWP image to demonstrate that Feige 55 was extremely metal-rich, particularly in Fe. Holberg et al. (1995b) later showed that the Feige 55 was actually a double degenerate system. The relatively long integration times, with respect to the 1.493 day orbital period, lead to considerable velocity smearing. We have co-added the spectra in the ISM frame and have also co-added the two relatively unsmeared stellar spectra obtained near quadrature (SWP 31178 and SWP 53873). Two very prominent and distinct ISM components are seen at $-14.2\,\mathrm{km\,s^{-1}}$ and $-59.3\,\mathrm{km\,s^{-1}}$ in Feige 55. The former is likely produced in the local ISM, while the latter, as suggested in Holberg, Tweedy, & Collins (1995), may be associated with dispersed nebular material at -15 km s^{-1}. The co-added stellar spectrum, which is at the system velocity, clearly shows individual lines due to Fe V, Fe VI, and Ni V.

PG 1210+533.—In contrast to the other DAO stars observed with *IUE*, Feige 55 and S216, PG 1210+533 shows no features other than a sharp He II λ1640 line. The IUESIPS version of the spectrum is discussed in Holberg et al. (1988).

GD 153.—This is a 40,000 K DA with a pure-H photosphere, which shares virtually the same ISM line as HZ 43. Only interstellar Si II λ1260, C II λ 1334, and O I λ1302 are detectable in our co-added spectrum.

GD 323.—This is a DAB star with a spectrum and energy distribution that have proved difficult to interpret (Koester,Liebert, & Suffer 1994 and references therein). Two SWP echelle spectra exist; however, one of them, SWP 40123, could not be satisfactorily processed by NEWSIPS software. We were unable to clearly identify any features with which to co-add these spectra.

HZ 43.—This well-known DA is one of the brightest EUV sources in the sky and lies along an interstellar line of sight of very low density. Barstow, Holberg, & Koester (1995) have used the *EUVE* spectrum of HZ 43 to set very low limits on He and other elements in the photosphere of this star. Not unexpectedly, we find no photospheric features and only extremely weak ISM lines. Our coadded spectrum is constructed from the four large-aperture spectra since we could not identify any lines in the small-aperture spectrum (SWP 27225).

EG 102.—This is a well-known 20,000 K DA star, frequently used as a flux and photometric standard. VTS first noted the presence of weak Si II $\lambda\lambda$1264, 1265 lines. The discovery of the Mg II λ4481 line in EG 102 (HBG), however, prompted a closer look at the single *IUE* SWP spectrum. They demonstrated that the excited Si II lines, including the 1309 Å and 1533 Å lines, had essentially the same velocity as the Mg II line and that of the stellar photosphere. The NEWSIPS spectrum also now shows the presence of Al II λ1670 and Al III $\lambda\lambda$1854, 1862, as well as a remarkably strong excited C II λ1335 line. The C II line, however, is blueshifted by 11 km s^{-1} from that of the stellar photosphere and differs appreciably from the other interstellar lines. We categorize the C II features as circumstellar. The remarkable aspect of the presence of Mg and Al in the photosphere of EG 102 is that residence time for downward diffusion for both these elements is on the order of only 3 days. This indicates that the star is subject to ongoing accretion of heavy elements from an unknown source. Main-sequence companions, of all temperatures, can be ruled out conclusively by IR photometry.

CD −38°10980.—This is a well-known bright DA star with a distant G5 V companion. The large number of SWP spectra is due to its use as an *IUE* calibration star. Holberg et al. (1985) first noted the presence of excited Si II and Si III lines, which suggests that these were photospheric. VTS later demonstrated that the Si abundances derived from these two ions were not consistent with a photospheric origin. A clearer picture of the nature of these features emerged from the work of HBA who used a co-added IUESIPS spectrum to demonstrate that these lines are formed in a dense photoexcited circumstellar environment near the stellar surface. The white dwarf photosphere itself is, to an exceptionally high degree, pure H. To date, no similar circumstellar features have been seen in other DA white dwarfs.

REJ 1629+780.—Like Feige 24 and REJ 1016−053, this DA is a member of a binary system containing a late-type M star showing variable strength Balmer emission lines. Sion et al. (1995) discussed the co-added IUESIPS spectrum of REJ 1629+780, finding no evidence of orbital motion or trace metals in the white dwarf photosphere. They attribute the variable emission lines to coronal activity in the M star. Our co-added spectrum remains consistent with these findings.

Wolf 1346.—At 20,000 K, Wolf 1346 is the coolest of the DA stars known to contain photospheric Si. The excited Si II $\lambda\lambda$1264, 1265 lines were first reported by Bruhweiler & Kondo (1983). The photospheric origin of these lines was confirmed by Holberg et al. (1996) who used a co-added *IUE* spectrum to demonstrate the presence of additional excited Si II lines as well as a set of weak excited Si III lines, all having a common velocity that matches the star's photospheric velocity. A Si abundance of log (Si/H) $= -7.5 \pm 0.2$ was determined and was shown to be comparable to the expected Si abundance due to radiative levitation.

GD 394.—Bruhweiler & Kondo (1983) first noted the exceptionally strong Si III and Si IV features in this 37,000 K DA star. Because of an apparent disagreement with a published GD 394 radial velocity and the velocity of the Si features, Bruhweiler & Kondo hypothesized that these lines

were circumstellar. This issue was resolved when Barstow et al. (1996) used *EUVE*, *GHRS*, and *IUE* echelle spectra to show that the Si (see Fig. 6) was photospheric and in large part explained the extremely large EUV opacity of GD 394. GD 394, however, remains an anomaly because of its extremely high Si abundance, log (Si/H) = −5.5. No other DA below 50,000 K has such a large value. Our co-added spectrum clearly shows the presence of previously undetected photospheric Al III λλ1854.74 and 1862.79 lines.

REJ 2214−491.—Like REJ 0623−374, REJ 2214−491 is an extremely metal-rich DA. Holberg et al. (1993) used both stars to establish the link between high levels of Fe and high EUV opacity in the hottest DA stars. Using a four-spectrum co-add, Holberg et al. found Ni in the spectrum of REJ 2214−491 (see Fig. 4), as did Werner & Driezler (1994).

GD 246.—VTS noted the presence of weak C IV, Si IV, and N V resonance lines in GD 246 and derived the abundances of these elements, under the assumption that these lines arose in the photosphere. Vennes et al. (1993) showed that this $T_{\rm eff}$ = 55,000 K DA has a highly cut off EUV spectrum, which implies a significant heavy element content in the photosphere. They also use a co-added NEWSIPS spectrum of GD 246 to estimate an ISM H I density from the saturated H I Lyα core. Our co-added spectrum reveals the C IV and Si IV resonance lines, but not N V or additional features.

REJ 2334−471.—This is a $T_{\rm eff}$ = 55,800 K DA falling in the high-opacity EUV temperature regime. Marsh et al. (1997) find evidence of such opacity in the *ROSAT* data. Our co-added spectrum shows the presence of C IV, Si IV, and N V resonance lines, presumably from the photosphere.

HD 223816B.—This is a DA + F5 IV system containing one of the hottest known DA stars at $T_{\rm eff}$ = 69,300 K (Barstow et al. 1996). These authors note the presence of strong EUV opacity; curiously we find only ISM lines in the stellar spectrum.

KPD 0005+511.—This is among the hottest and most peculiar of the DO stars. Although its photospheric $T_{\rm eff}$ is only 120,000 K, it shows high excitation O VIII emission lines and is the only white dwarf known to possess an X-ray corona (Fleming, Werner, & Barstow 1993). Fritz et al. (1990a) found evidence of far-UV resonance lines (C IV, Si IV, and N V) at a velocity different from the ISM lines and suggested they originated in a circumstellar photoionized H II region near the star. Sion et al. (1997) used a co-added SWP echelle spectrum of KPD 0005+511 to add to the discoveries of Werner et al. (1996) and Dreizler et al. (1998) who observed several portions of the star's UV spectrum with the GHRS. The only unambiguous photospheric features found are due to N V λλ1238, 1242, C IV λ1230 and He II λ1640. Nonphotospheric blueshifted lines due to the N V, C IV, and Si IV resonance lines are clearly present, displaced approximately 40 km s^{-1} from the photospheric velocity. Sion et al. present evidence of spectral variability in the N V lines. An intriguing aspect of the interstellar line of sight to KPD 0005+511 is the presence of C I lines, indicating a foreground diffuse cloud along this sight line. Sion et al. speculate that this cloud, if near KPD 0005+511, could interact with the stellar wind to produce a zone of shock-induced ionization. An alternative view of the sight line to KPD 0005+5106 is given by Kruk & Werner (1998) whose Hopkins Ultraviolet Telescope (HUT) spectrum of this star reveals strong molecular H_2 absorption below 1200 Å and is postulated as evidence of an old planetary nebula.

NGC 246.—This is the central star of the planetary nebula NGC 246 and a prime example of an O VI central star. Feibelman (1995) and Feibelman & Johansson (1995) present a detailed inventory of the features present in a co-added IUESIPS spectrum of this star. They find numerous excited C IV and O VI absorption features, as well as broad P Cygni profiles for the C IV resonance lines. Rauch & Werner (1998) have used co-added *IUE* spectra of NGC 246 and NLTE model atmospheres to derive H, C, and O abundances for this star. Our co-added NEWSIPS spectrum confirms many of these lines, in particular numerous excited asymmetrical C IV lines with shallow blue wings. The velocity of the photosphere, defined by the O V λ1371 and two excited C IV lines, is -22 ± 1.2 km s^{-1}. Also present is a well-defined blueshifted component at -70.2 ± 1.1 km s^{-1} in the N V, C IV, and Si IV resonance features. We find no evidence of the Fe VII features reported by Feibelman & Bruhweiler (1990).

REJ 0503−289.—This is a bright $T_{\rm eff}$ = 70,000 K DO star and a strong long wavelength EUV source having a very low interstellar H II column density (Barstow et al. 1994a). The only previous discussion of the *IUE* echelle data from this star is that of Barstow & Sion (1994), who present evidence, from two IUESIPS spectra (SWP 46428 and SWP 49788) taken more than one year apart, of variable C IV, O V, and He II features. They suggest this is evidence of episodic mass loss. Our co-added spectrum clearly shows evidence of blueshifted components in the N V and C IV resonance lines. Moreover, a comparison of the individual spectra shows very good evidence of variability in the blueshifted C IV features. These observations in combination with GHRS observations of REJ 0503−289 will be discussed in more detail elsewhere.

PG 1034+001.—The intermediate-temperature DO star PG 1034+001 was observed by Sion, Liebert, & Wesemael (1985) who found photospheric features due to the N V and C IV doublets and the O V λ1371 line. Fritz et al. (1990a) detected the Si IV λ1400 resonance lines and noted a curious double structure in the lines. Our co-added spectrum presents a clearer picture. Si IV is clearly present at two distinct velocity components, +51 km s^{-1} and +7 km s^{-1}. This two-component characteristic is also seen in the C IV lines. Following Sion, Liebert, & Wesemael, we identify the +51 km s^{-1} with the stellar photosphere and the blueshifted component with a weak stellar wind. We also note the He II λ1640 line is located at an intermediate velocity of +24 km s^{-1}, which is likely to be a result of blending of the photospheric and blueshifted components. Dreizler et al. (1998) have analyzed GHRS spectra of PG 1034+001, finding good evidence of Fe VI and Fe VII in the spectrum of this star, first reported by Feibelman & Bruhweiler (1990). Dreizler et al., however, attribute the blueshifted C IV and Si IV features to the ISM. We confirm the features found by Dreizler et al. but note a systematic 20 km s^{-1} difference in the velocities obtained by these authors and our results. In addition, we find a statistically significant difference between the ISM velocity and that of the blueshifted components.

PG 1159−035.—This star is the prototype of the class of hot pulsating variable He-rich white dwarfs. Liebert et al. (1989) analyzed a single SWP echelle spectrum of PG 1159−035 finding a number of highly ionized features,

including N v λ1240 and C iv λ1550 resonance lines, O v λ1371, and highly excited C iv lines. No conclusive evidence of mass loss or winds was found by either Liebert et al. or by Fritz et al. (1990a). Our co-added spectrum clearly reveals blueshifted components in the N v and C iv resonance lines (see Fig. 8).

HZ 21.—At 50,000 K, HZ 21 is one of the coolest of the DO stars. Fritz et al. (1990b) analyzed the IUESIPS version of this spectrum, finding a spectrum rich in ISM lines but with no evidence of stellar features, other than a curiously shaped He ii λ1640 feature. Our NEWSIPS spectrum largely confirms these results; however, the He ii feature is not included in Table 4 owing to ambiguity regarding its extent.

HD 149499B.—The hot DO star HD 149499B is a member of a binary system with a KO V primary and thus is observable only at UV wavelengths. Sion & Guinan (1983) used the He ii λ1640 and the C iv doublet to obtain a gravitational redshift for HD 149499B. Our co-added spectrum of HD 149499B shows new aspects of its spectrum. These include weak Si iv $\lambda\lambda$1393, 1402 lines that share the radial velocity of the C iv lines and are curiously 18 km s^{-1} redshifted with respect to an asymmetrical He ii line. If the C iv and Si iv lines are regarded as photospheric, the He ii λ1640 line could well possess a blueshifted component.

GD 358.—This is one of the two He-rich DB stars observed with *IUE* in echelle mode. Sion et al. (1989) present a co-addition of the two IUESIPS spectra of this star showing photospheric features, a modest He ii λ1640 line, and lines due to C ii $\lambda\lambda$1334 and 1335. Provencal et al. (1996) discuss GHRS spectra of GD 358 covering several regions between 1200 and 1655 Å. They confirm the *IUE* results and determine a carbon abundance that suggests convective mixing as the source of the C in the photosphere of this DB star. They also find a small hydrogen abundance. Our co-added NEWSIPS spectrum shows no new features.

K1-16.—This is a very hot DOZ star having a planetary nebula central of PG 1159 spectral type. Feibelman & Bruhweiler (1990) have reported possible Fe vii lines in the existing NEWSIPS spectrum. The NEWSIPS spectrum shows N v, Si iv, and C iv resonance lines at a velocity of -48 km s^{-1} but no evidence of any Fe vii lines at this velocity. The ISM lines exhibit two components at -20 and -48 km s^{-1}.

RXJ 2117.1+3412.—This is an extremely hot ($T_{\rm eff}$ = 170,000 K) hydrogen-deficient planetary nebula central star of PG 1159 spectral type. GHRS observations of this star are discussed in Werner et al. (1996), where they discuss a number of highly excited C iv and O vi photospheric absorption features and several broad emission features due to O viii, C v, and N v. The latter cannot be produced in the photosphere and are postulated to be due to collisions in a wind. Rauch & Werner (1998) employed NLTE model atmospheres of co-added *IUE* spectra of RXJ 2117.1+3412 to determine the effective temperature, gravity and He:C:O ratios for this star. A number of broad lines due to highly excited C iv and O vi transitions are identified by Rauch & Werner. Our co-added spectrum reveals many of the same excited C iv features as Werner et al. Although these features are diffuse and difficult to accurately measure, we find a photospheric velocity of $+47.2$ km s^{-1}. In addition we also find a set of N v, C iv, and Si iv resonance lines at -11.9 km s^{-1}, which we identify as circumstellar. Werner et al. classify these N v features as interstellar.

4.2. *Summary*

We have presented a uniform analysis of the echelle spectra of the hot white dwarfs, as well as several planetary nebula central stars, contained in the *IUE* archives. For almost all of these, it is the first time NEWSIPS versions of the data have been analyzed and discussed. We list the interstellar, stellar, and circumstellar features found in the spectra and present a discussion of our data reduction procedures and some of the improvements represented by NEWSIPS data over the previous IUESIPS versions. We also discuss corrections to the wavelength scale and the uncertainty vector we have found it necessary to make to the NEWSIPS data. Further work on the abundances and abundance upper limits for various heavy elements in white dwarf photospheres derived from these data will be presented elsewhere.[4]

The former *IUE* Data Analysis Center (IUEDAC) and the National Space Science Data Center (NSSDC) are acknowledged for providing the archive NEWSIPS spectra presented here. We are deeply indebted to Myron Smith and Joy Nichols for many valuable discussions regarding NEWSIPS data. We also wish to thank Jim Collins and David Sing for the considerable effort they devoted to the reduction of the NEWSIPS spectra and the reviewer, James Liebert, for suggesting several valuable additions to this paper. J. B. H. wishes to acknowledge support from NASA grants NAG 5−3472 and NAG 5−2738. M. A. B. acknowledges support of PPARC, UK. E. M. S. acknowledges support by NSF grant AST 90-16283-A01

[4] Reduced versions of all the spectra discussed in this paper, including co-added spectra, are available electronically in FITS format via the world wide web at ftp vega.lpl.arizona.edu/newsips.

REFERENCES

Barstow, M. A., et al. 1993, MNRAS, 264, 16
Barstow, M. A., Holberg, J. B., Cruise, A. M., & Penny, A. J. 1997, MNRAS, 290, 505
Barstow, M. A., Holberg, J. B., Fleming, T. A., Marsh, M. C., Koester, D., & Wonnecott, D. 1994a, MNRAS, 270, 499
Barstow, M. A., Holberg, J. B., Hubeny, I., Lanz, T., Bruhweiler, F. C., & Tweedy, R. W. 1996, MNRAS, 279, 1120
Barstow, M. A., Holberg, J. B., & Koester, D. 1995, MNRAS, 274, L31
Barstow, M. A., Holberg, J. B., Werner, K., Buckley, D. A. H., & Stobie, R. S. 1994b, MNRAS, 267, 653
Barstow, M. A., Hubeny, I., & Holberg, J. B. 1998, MNRAS, submitted
Barstow, M. A., & Sion, E. M. 1994, MNRAS, 271, L52
Bergeron, P., Saffer, R. A., & Liebert, J. 1992, ApJ, 394, 228
Bergeron, P., Wesemael, F., Beauchamp, A., Wood, M. A., Lamontagne, R., Fontaine, G., & Liebert, J. 1994, ApJ, 432, 305.
Bruhweiler, F. C. 1984, in Future of Ultraviolet Astronomy Based on Six Years of *IUE* Research, ed. J. M. Mead, Y. Kondo, & R. Chapman (NASA CP-2349), 269
Bruhweiler, F. C., & Kondo, Y. 1981, ApJ, 248, L123
———. 1982, ApJ, 259, 232
———. 1983, ApJ, 269, 657
Bruhweiler, F. C., & Sion, E. M. 1986, ApJ, 304, L21
Bruhweiler, F. C., & Vidal-Madjar, A. 1987, in Exploring the Universe with the *IUE* Satellite, ed. Y. Kondo (Dordrecht: Reidel), 467
Chayer, P., Fontaine, G., & Wesemael, F. 1995, ApJS, 99, 189

Dreizler, S., Werner, K., Heber, U., & Reid, N. 1998, in Proc. of the 3rd Conference on Faint Blue Stars, ed. A. G. D. Philip, J. Liebert, & R. A. Saffer (Schenectady: Davis), in press
Dupree, A. K., & Raymond, J. C. 1982, ApJ, 263, L63
Feibelman, W. A. 1995, PASP, 107, 531
Feibelman, W. A., & Bruhweiler, F. C. 1990, ApJ, 357, 548
Feibelman, W. A., & Johansson, S. 1995, ApJS, 100, 405
Feibelman, W. A., Kaler, J. B. Bond, H. E., & Graurer, A. D. 1995, PASP, 107, 914
Finley, D. S., Koester, D., & Basri, G. 1997, ApJ, 488, 375
Fleming, T. A., Werner, K., & Barstow, M. A. 1993, ApJ, 416, L79
Fritz, M. L., Leckenby, H. J., & Sion, E. M. 1990a, AJ, 99, 908
Fritz, M. L., Leckenby, H., Sion, E. M., Vauclair, G., & Liebert, J. 1990b, AJ, 99, 668
Garhart, M. P. 1993, NASA *IUE* Newsletter, No. 51, 1
Guinan, E. F., Wacker, S. W., Baliunas, S. L., Loesser, J. G., & Raymond, J. 1986, in New Insights in Astrophysics (ESA SP-263) (Paris: ESA), 197
Hipparcos Catalog. 1997, The Hipparcos and Tycho Catalogs (Noordwijk: ESA)
Hodgkin, S. T., Barstow, M. A., Fleming, T. A., Monier, R., & Pye, J. P. 1993, MNRAS, 263, 229
Holberg, J. B. 1995, in Lecture Notes in Physics 443, White Dwarfs, ed. D. Koester & K. Werner (Berlin: Springer), 138
Holberg, J. B., et al. 1993, ApJ, 416, 806
Holberg, J. B., Barstow, M. A., Bruhweiler, F. C., & Collins, J. 1996, AJ, 111, 2361
Holberg, J. B., Barstow, M. A., Bruhweiler, F. C., Cruise, A. M., & Penny, A. J. 1998a, ApJ, 497, 935
Holberg, J. B., Barstow, M. A., Bruhweiler, F. C., & Sion, E. M. 1995a, ApJ, 453, 313
Holberg, J. B., Barstow, M. A., Burleigh, M., & Sion, E. M. 1998b, in preparation
Holberg, J. B., Barstow, M. A., & Green, E. M. 1997, ApJ, 474, L127 (HBG)
Holberg, J. B., Barstow, M. A., Lanz, T., & Hubeny, I. 1997, ApJ, 484, 871
Holberg, J. B., Barstow, M. A., & Sion, E. M. 1998c, in The Third Conference on Faint Blue Stars, ed. A. D. G. Philip, R. Saffer, & J. Liebert, (Schenectady: Davis), in press
———. 1998d, in Ultraviolet Astrophysics Beyond the *IUE* Final Archive, ed. W. Wamsteke, R. González-Riesha, & R. A. Harris (ESA SP 413), 237
Holberg, J. B., Bruhweiler, F. C., & Andersen, J. 1995a, ApJ, 443, 753 (HBA)
Holberg, J. B., Hubeny, I., Barstow, M. A., Lanz, T., Sion, E. M., & Tweedy, R. W. 1994, ApJ, 425, L105
Holberg, J. B., Saffer, R. A., Tweedy, R. W., & Barstow, M. A. 1995b, ApJ, 452, L133
Holberg, J. B., Sion, E. M., Liebert, J., & Vauclair, G. 1988, in A Decade of UV Astronomy with *IUE* (ESA SP-281), 1, 263
Holberg, J. B., Tweedy, R. W., & Collins, J. 1995, in Lecture Notes in Physics 443, White Dwarfs, ed. D. Koester & K. Werner (Berlin: Springer), 202
Holberg, J. B., Wesemael, F., Wegner, G., & Bruhweiler, F. C. 1985, ApJ, 293, 294
Jelinsky, P. N. 1988, Ph.D. thesis, Univ. of California, Berkeley
Jordan, S., Napiwotzki, R., Koester, D., & Rauch, T. 1997, A&A, 318, 416
Kelly, R. L., & Palumbo, I. J. 1973, Atomic and Ionic Emission Lines below 2000 Angstroms (NRL Report 7599)
Kidder, K. M. 1991, Ph.D. thesis, Univ. of Arizona
Koester, D., Liebert, J., & Suffer, R. A. 1994, ApJ, 422, 783
Kruk, J. W., & Werner, K. 1998, ApJ, 502, 858
Lamontagne, R., Wesemael, F., Bergeron, P., Liebert, J., Fulbright, M. S., & Green, R. F. 1993, in White Dwarfs: Advances in Observation and Theory, ed. M. A. Barstow (Dordrecht: Kluwer), 347
Lanz, T., Barstow, M. A., Hubeny, I., & Holberg, J. B. 1996, ApJ, 473, 1089
Lemoine, M., Vidal-Madjar, A., Bertin, P. Ferlet, R., Gry, C., & Lallement, R. 1996, A&A, 308, 601
Liebert, J., Wesemael, F., Husfeld, D., Wehrse, R., Starrfield, S. G., & Sion, E. M. 1989, AJ, 97, 1440
Marsh, M. C., et al. 1997, MNRAS, 287, 705
McCook, G. P., & Sion, E. M. 1998, ApJS, in press
Morton, D. C. 1991, ApJS, 77, 119
Mullan, D. J., Shipman, H. L., Sion, E. M., & MacDonald, J. 1991, ApJ, 374, 707
Mullan, D. J., Sion, E. M., Bruhweiler, F. C., & Carpenter, K. G. 1989, ApJ, 339, L33
Nichols, J. S., & Linsky, J. L. 1996, AJ, 111, 517
O'Donoghue, D., Chen, A., Killkenny, D., & Stobie, R. S. 1993, in White Dwarfs: Advances in Observation and Theory, ed. M. A. Barstow (Dordrecht: Kluwer), 39
Provencal, J. L., Shipman, H. L., Thejll, P., Vennes, S., & Bradley, P. A. 1996, ApJ, 466, 1011
Rauch, T., & Werner, K. 1998, in Proc. of the 3rd Conference on Faint Blue Stars, ed. A. G. D. Philip, J. Liebert, & R. A. Saffer (Schenectady: Davis), in press
Shipman, H. L. 1984, in Future of Ultraviolet Astronomy Based on Six Years of *IUE* Research, ed. J. M. Mead, Y. Kondo, & R. Chapman (NASA CP-2349), 281
Sion, E. M., Bohlin, R. C., Tweedy, R. W., & Vauclair, G. P. 1992, ApJ, 391, L29
Sion, E. M., Bruhweiler, F. C., Mullan, D., & Carpenter, K. 1989, ApJ, 341, L17
Sion, E. M., & Guinan, E. F. 1983, ApJ, 265, L87
Sion, E. M., Holberg, J. B., Barstow, M. A., & Kidder, K. M. 1995, PASP, 107, 232
Sion, E. M., Holberg, J. B., Barstow, M. A., & Scheible, M. P. 1997, AJ, 113, 364
Sion, E. M., Liebert, J., Vauclair G., & Wegner, G. 1989, in IAU Collq. 114, White Dwarfs, ed. G. Wegner (Berlin: Springer), 354
Sion, E. M., Liebert, J., & Wesemael, F. 1985, ApJ, 292, 477
Sion, E. M., Schaefer, K. G., Bond, H. E., Saffer, R. A., & Cheng, F. H. 1998, ApJ, 496, L29
Smith, M. 1998, STSci Archive Newsletter, Vol. 3
Stys, D. et al. 1999, in preparation
Thorstensen, J. R., Vennes, S., & Bowyer, S. 1996, ApJ, 457, 390
Tweedy, R. W. 1991, Ph.D. thesis, Univ. of Leicester
———. 1993, in White Dwarfs: Advances in Observations and Theory, ed. M. A. Barstow (Dordrecht: Kluwer), 317
Tweedy, R. W., & Napiwotzki, R. 1992, MNRAS, 259, 315
van Altena, W. F., Lee, J. T., & Hoffleit, D. 1991, Yale General Catalogue of Trigonometric Stellar Parallaxes (New Haven, Yale Univ. Obs.)
Vauclair, G., Vauclair, S., & Greenstein, J. L. 1979, A&A, 80, 79
Vennes, S., Chayer, P., Hurwitz, M., & Bowyer, S. 1996, ApJ, 468, 898
Vennes, S., Chayer, P., Thorstensen, J. R., Bowyer, C. S., & Shipman, H. L. 1992, ApJ, 392, L27
Vennes, S., Christian, D. J., & Thorstensen, J. R. 1998, preprint
Vennes, S., Dupuis, J., Rumph, T., Drake, J., & Bowyer, S. 1993, ApJ, 410, L119
Vennes, S., Thejll, P., Galvan, R. G., & Dupuis, J. 1997, ApJ, 480, 714
Vennes, S., Thejll, P., & Shipman, H. L. 1991, in 7th European Workshop on White Dwarfs: White Dwarfs, ed. G. Vauclair & E. Sion (Dordrecht: Kluwer), 235 (VTS)
Vennes, S., & Thorstensen, J. R. 1994, AJ, 108, 1881
Vennes, S., & Thorstensen, J. R., Thejll, P., & Shipman, H. L. 1991, ApJ, 372, L37
Webbink, R. F., Guinan, E. F., Koch, R. H., Kondo, Y., Etzel, P. B., & Thrash, T. A. 1992, BAAS, 24, 1127
Wiese, W. L., Smith, M. W., & Glennon, B. M. 1966, Atomic Transition Probabilities: Hydrogen through Neon (NSRD-NBS 4) (Washington, DC: GPO)
Werner, K., & Dreizler, S. 1994, A&A, 286, L31
Werner, K., Dreizler, S., Heber, U., Kappelmann, N., Kruk, J., Rauch, T., & Wolff, B. 1997, Rev. Mod. Astron., 10, 219
Werner, K., Dreizler, S., Heber, U., Rauch, T., Fleming, T. A., Sion E. M., & Vauclair, G. 1996, A&A, 307, 860
Werner, K., Hamann, W.-R., Heber, U., Napiwotzki, R., Rauch, T., & Wessolowski, U. 1992, A&A, 259, L68
Wolff, B., Koester, D., Dreizler, S., & Hass, S. 1998, A&A, 329, 1045
Zuckerman, B., & Reid, I. N. 1998, ApJ, 505, L00